Modeling and analysis of the tritium fuel cycle for ARC- and STEP-class D-T fusion power plants

PAPER • OPEN ACCESS

Modeling and analysis of the tritium fuel cycle for ARC- and STEP-class D-T fusion power plants

OPEN ACCESS
IOP Publishing | International Atomic Energy Agency
Nuclear Fusion
Nucl. Fusion **63** (2023) 126005 (34pp)
https://doi.org/10.1088/1741-4326/acf3fc

Modeling and analysis of the tritium fuel cycle for ARC- and STEP-class D-T fusion power plants

Samuele Meschini[1], Sara E. Ferry[2,*], Rémi Delaporte-Mathurin[2] and Dennis G. Whyte[2]

[1] Dipartimento Energia 'Galileo Ferraris', Politecnico di Torino, Corso duca degli abruzzi 24, Turin, Italy
[2] Plasma Science and Fusion Center, Massachusetts Institute of Technology, Cambridge, MA 02139, United States of America

E-mail: seferry@mit.edu

Received 13 June 2023, revised 9 August 2023
Accepted for publication 25 August 2023
Published 14 September 2023

Abstract

The limited tritium resources available for the first fusion power plants (FPPs) make fuel self-sufficiency and tritium inventory minimization leading issues in FPP design. This work builds on the model proposed by Abdou *et al* (2020 *Nucl. Fusion* **61** 013001), which analyzed the fuel cycle (FC) of a DEMOnstration nuclear FPP-class FPP with a time-dependent system-level model. Here, we use a modified version of their model to analyze the FC of an Affordable, Robust, Compact (ARC)-class tokamak and two versions of a Spherical Tokamak for Energy Production (STEP)-class tokamak. The ARC-class tokamak breeds tritium in a 2LiF + BeF_2 liquid immersion blanket, while the STEP-class tokamak breeds tritium utilizing either a liquid-lithium blanket design or an encapsulated breeding blanket. A time-dependent system-level model is developed in Matlab Simulink® to simulate the evolution of tritium flows and tritium inventories in the FC. The main goals of this work are to assess tritium self-sufficiency of the ARC- and STEP-class designs and to determine quantitative design requirements that can be used to analyze the adequacy of a proposed FC system. These design requirements are aimed at achieving a low tritium inventory doubling time (t_d) and a low start-up inventory ($I_{startup}$) while keeping the required tritium breeding ratio (TBR_r) as low as possible. We also consider how improvements in FC technology and POs affect TBR_r and $I_{startup}$. The model results show that TBR_r for ARC- and STEP-class FPPs should be achievable if the tritium burn efficiency (TBE) reaches 0.5%–1% ($TBR_r < 1.2$). This assumes significant, but attainable, improvements over current abilities. However, the model results indicate that an FPP must achieve ambitious performance targets, including FPP availability >70%, tritium processing time <4 h, and the implementation of direct internal recycling (DIR). If future research yields major improvements to achievable TBE, it may be possible to achieve tritium self-sufficiency while operating at lower availability and without implementing DIR.

* Author to whom any correspondence should be addressed.

Keywords: ARC, STEP, FPP, fusion fuel cycle, tritium self-sufficiency, tritium inventories, tritium breeding

(Some figures may appear in colour only in the online journal)

1. Introduction

The Affordable, Robust, Compact (ARC) FPP [2] and the Spherical Tokamak for Energy Production (STEP) [3, 4] are conceptual fusion power plant (FPP) designs being developed by Commonwealth Fusion Systems (U.S.) and the UKAEA (U.K.) respectively. ARC is an example of the compact, toroidal FPP class, with an assumed fusion power $P_{fus} = 525\,MW_{th}$ and major radius $R = 3.3\,m$. STEP research teams have proposed three different spherical tokamak (ST) designs, with a major radius ranging from 3.26 m (compact design) to 5 m (DEMO-like design), and a fusion power $P_{fus} = 3300\,MW_{th}$ [4].

ST designs arose from studies of alternative tokamak configurations that featured low aspect ratios [5–7], culminating in the development of experimental ST designs (e.g. START, MAST) [8] and ST concepts for energy production (e.g. STEP [9]). The ARC design came from considering the high power density enabled by high temperature superconducting magnets. This led to a novel design in which the vacuum vessel (VV) is inside the blanket, which itself is a large tank of molten $2LiF + BeF_2$ (FLiBe) salt referred to as the liquid immersion blanket (LIB). This enables maximum volumetric coverage of the neutron source by the breeder material. It also provides efficient heat conduction away from the coupled first wall (FW)-VV structure, which is very important at the high power density ARC proposes. Analyses of ARC have been carried out in the fields of materials science [10–12], thermal analysis [13–15], neutronics [13, 16–18], and plasma physics [2, 13, 19].

The goal of this work is to carry out a dynamic analysis of the fuel cycles (FCs) of ARC- and STEP-class FPPs, which have yet to be investigated in the literature.

Tritium self-sufficiency refers to the ability of an FPP to breed, process, and use its own tritium (T) fuel while producing sufficient excess tritium to maintain the desired reserve inventory (used in the event that some part of the FC ceases operation) and to contribute to $I_{startup}$ for subsequent FPPs. Tritium self-sufficiency of FPPs [1, 20] is expected to be a significant challenge in FPP design and operation. Abdou *et al* [1] showed that tritium self-sufficiency may be extremely challenging or even impossible for proposed DEMOnstration power plant (DEMO) designs. For a fueling efficiency $\eta_f \approx 25\%$ (obtained by extrapolating from DIII-D studies [21] to DEMO) and a burn fraction $f_b = 0.36\%$ (the expected achievable value in ITER, assuming two pellet injectors with a maximum fueling rate of $120\,Pa\,m^3\,s^{-1}$ [22]), the tritium breeding ratio required (TBR_r) to achieve tritium self-sufficiency in DEMO will be 1.82. This is far above its maximum achievable TBR (TBR_a), which is expected to range from 1.1 to 1.2 depending on the chosen blanket design [23]. Relying on external tritium supplies is not a sustainable option, as global inventory is highly constrained. Most of the World's tritium supply is produced by CANadian Deuterium Uranium (CANDU) reactor operations [20, 24]. The available tritium supply from CANDU reactors is expected to peak at ≈27 kg in 2027 [1]. The peak may be higher (up to ≈40 kg) if additional tritium is made available by the operating and planned heavy water reactors outside Canada (e.g. in Romania and the Republic of Korea [20, 24]).

No other significant tritium sources are expected to come online in the near future [20]. ITER plans to start D-T operations in the late 2030s and will consume approximately 12.3 kg of tritium during its planned experimental campaigns, leaving ≈15 kg of theoretically available tritium for the startup of FPPs that begin operation after 2050 [20, 24]. Therefore, minimizing $I_{startup}$ and ensuring the robustness and efficiency of tritium breeding and extraction systems will be of paramount importance for the first non-ITER D-T fusion devices. In this regard, our analysis aims at (1) assessing tritium self-sufficiency in ARC and STEP; (2) quantifying tritium inventories and tritium flows between FC components, with and without the implementation of direct internal recycling (DIR); and (3) providing quantitative design targets for ARC and STEP that achieve a low t_d and a low $I_{startup}$.

1.1. Understanding fueling efficiency (η_f), burn fraction (f_b), and tritium burn efficiency (TBE)

Consider a very high-level, simplified view of the fueling process. Tritium (T) and deuterium (D) fuel is injected into the vacuum chamber of a DT-burning FPP. If the tritium is burned in the plasma, it produces high-energy neutrons and heat that pass to the blanket, and charged alpha particles (referred to as helium ash) that contribute to plasma heating and which are eventually exhausted from the divertor. Unburned tritium is eventually exhausted from the divertor as a neutral particle, reused as fuel via DIR [25], or re-processed in the tritium plant[3]. In [1], the most important parameter used to characterize the FC is the product of the fueling efficiency η_f and burn fraction f_b. Here, we will briefly review these terms and explain why we believe the concept of tritium burn efficiency (TBE) is the more illustrative parameter.

[3] The same can be said for deuterium, but deuterium is not a limited resource and can be readily obtained, which is why it is largely ignored in these discussions.

The fueling efficiency is defined in [1] as the ratio of the tritium fueling rate to the tritium injection rate[4]:

$$\eta_{\mathrm{f}} = \frac{\dot{T}_{\mathrm{fuel}}}{\dot{N}_{\mathrm{T,in}}}. \tag{2}$$

where $\dot{T}_{\mathrm{fuel}}$ is defined by [1] as the rate of injected tritium that enters and penetrates the plasma and $\dot{N}_{\mathrm{T,in}}$ is the tritium injection rate in the vacuum chamber. Some fraction of the injected tritium that successfully penetrates the plasma is burned in a DT fusion reaction. This is the burn fraction f_{b}:

$$f_{\mathrm{b}} \equiv \frac{\dot{N}_{\mathrm{T,burn}}}{\dot{T}_{\mathrm{fuel}}}. \tag{3}$$

The remainder loses confinement and is transported out of the core plasma before it can undergo a fusion reaction. Therefore, the total amount of tritium that undergoes a fusion reaction is expressed in [1] as the product $\eta_{\mathrm{f}} f_{\mathrm{b}}$. In [1], any injected tritium that loses confinement before undergoing fusion is directly exhausted by the divertor.

However, this is not a completely accurate way to characterize the fueling process. Unburned T is not immediately exhausted. Instead, an injected tritium particle undergoes many neutralization and ionization processes in the divertor and can re-enter the core plasma multiple times before finally being exhausted [26, 27]. This has important implications for how we understand fueling efficiency in an FPP. Consider the vacuum chamber as the boundary of the system of interest, containing both the core plasma and the divertor plasma regions. Particles enter this system via fueling injection, and particles exit this system via divertor exhaust (with a fraction undergoing fusion reactions or being lost in the walls). Within the vacuum boundary, particles can be exchanged between the divertor and core plasma regions. Now, apply equilibrium conditions to particle populations in the system. Burning tritium, exhausting helium ash, and exhausting unburned fuel affect this equilibrium. The assumption that unburned tritium is immediately exhausted has a significant impact on our assessment of the particle equilibria in the FPP vacuum boundary. We must account for the realistic steady-state equilibrium scenario, in which particles are exchanged between the core and divertor regions many times without leaving the vacuum boundary, in order to understand the maximum efficiency at which we can burn tritium fuel. To do this, we introduce the concept of TBE which is derived in detail in [27] and summarized briefly here.

TBE is defined as:

$$\mathrm{TBE} \equiv \frac{\dot{N}_{\mathrm{T,burn}}}{\dot{N}_{\mathrm{T,in}}}. \tag{4}$$

[4] More fundamentally, η_{f} can be described as

$$\eta_{\mathrm{f}} = \frac{\Delta N_{e,\mathrm{pl}}}{N_{e,\mathrm{inj}}} \tag{1}$$

where $N_{e,\mathrm{pl}}$ is the number of electrons in the plasma and $N_{e,\mathrm{inj}}$ is the number of electrons injected in the fuel. If fueling efficiency is high, the injection of fuel leads to a significant increase in the electron density of the plasma after the fueling event [1].

where $\dot{N}_{\mathrm{T,burn}}$ is the tritium burn rate[5]. The TBE should not be confused with the definition of tritium burn fraction given in [1] (equation (3)).

Mathematically speaking, TBE $= \eta_{\mathrm{f}} f_{\mathrm{b}}$, which is the key parameter used in [1]. Nevertheless, the definitions of η_{f} (equation (2)) and f_{b} (equation (3)) assume that tritium particles that do not penetrate the plasma, or which penetrate but do not burn, are directly exhausted by the divertor pumps. This can be a misleading assumption, especially when considering the link between TBE and core/divertor physics.

Taking the VV as the system boundary and assuming that the system tritium inventory remains constant, tritium fueling is required to balance the tritium loss due to burning in the plasma and exhaust of unburned tritium from the divertor ($\dot{N}_{\mathrm{T,div}}$):

$$\dot{N}_{\mathrm{T,in}} = \dot{N}_{\mathrm{T,burn}} + \dot{N}_{\mathrm{T,div}}. \tag{5}$$

Combining equations (4) and (5) one obtains:

$$\mathrm{TBE} = \frac{\dot{N}_{\mathrm{T,burn}}}{\dot{N}_{\mathrm{T,burn}} + \dot{N}_{\mathrm{T,div}}}. \tag{6}$$

From equation (6) the relationship between TBE and the unburned fuel exhausted from the divertor is evident. $\dot{N}_{\mathrm{T,div}}$ must be reduced to achieve large TBE. Nevertheless, exhaust pumping must be carefully optimized to avoid excessive helium ash dilution of the fuel.

The D-T fusion reaction produces a high energy neutron and alpha particle. The production of the latter results in helium ash dilution of the plasma, which is defined as:

$$f_{\mathrm{dil}} \equiv \frac{n_\alpha}{n_e} \tag{7}$$

where n_α and n_e are respectively the density of helium ash and electrons in the plasma. We must therefore consider the terms in equation (6) more closely.

The tritium burn rate is equal to the alpha particle production rate in the core plasma, $\dot{N}_\alpha$. The helium-to-fuel fraction in the core plasma is defined as the ratio of helium ash density to fuel ion density:

$$f_{\alpha,\mathrm{core}} = \frac{n_{\alpha,\mathrm{core}}}{n_{Q,\mathrm{core}}} \tag{8}$$

where Q denotes fuel species (DT, T_2, D_2).The ash dilution fraction is related to the helium-to-fuel fraction:

$$f_{\mathrm{dil}} = \frac{n_\alpha}{n_e} = \frac{f_{\alpha,\mathrm{core}}}{1 + 2 f_{\alpha,\mathrm{core}}}. \tag{9}$$

f_{dil} sets an important constraint on the helium ash density in the core. In fact, the fusion power decreases as the ash dilution fraction increases [27]:

$$\frac{P_{\mathrm{f}}}{P_{\mathrm{f,max}}} = (1 - 2 f_{\mathrm{dil}})^2 \tag{10}$$

[5] Unless otherwise specified, we assume that the fusion power and the tritium burn rate are constant FPP parameters.

where P_f is the fusion power density and $P_{f,max}$ is the fusion power density when $f_{dil} = 0$. Keeping a low ash concentration (i.e. a low dilution fraction) is therefore mandatory to avoid a detrimental reduction of the fusion power density.

Divertor pumps fulfill this function by removing helium ash from the divertor at an exhaust rate $\dot{N}_{He,div}$. At steady state, $\dot{N}_{He,div}$ equals the α particle production rate in the core plasma. Therefore:

$$\dot{N}_{T,burn} = \dot{N}_{\alpha} = \dot{N}_{He,div}. \tag{11}$$

Combining equation (6) with equation (11) we find:

$$TBE = \frac{\dot{N}_{He,div}}{\dot{N}_{He,div} + \dot{N}_{T,div}}. \tag{12}$$

Next, we relate TBE to divertor parameters. We define the helium-to-fuel fraction in the divertor as:

$$f_{He,div} = \frac{n_{He,div}}{n_{Q,div}} \tag{13}$$

The divertor pumping rate of species x is given as:

$$\dot{N}_{x,div} = n_{x,div} S_x \tag{14}$$

where n_x is the neutral gas density and S_x is the effective pumping speed. Next, we define the ratio of pumping speeds for helium and for all the unburned fuel species from the divertor:

$$\Sigma = \frac{S_{He}}{S_Q}. \tag{15}$$

By substituting equations (13)–(15) in equation (12) we arrive at:

$$TBE = \left(\frac{1}{2 f_{He,div} \Sigma} + 1\right)^{-1} \tag{16}$$

where we considered a 50/50 DT mixture in the plasma such that:

$$\dot{N}_{T,div} = \dot{N}_{D,div} = \frac{1}{2}\dot{N}_{Q,div} \tag{17}$$

where $\dot{N}_{D,div}$ is the deuterium exhaust rate and $\dot{N}_{Q,div}$ is the hydrogenic species exhaust rate. A useful parameter to link the helium fraction present in the core and in the divertor is the helium enrichment coefficient, defined as:

$$\eta_{He} = \frac{f_{He,div}}{f_{\alpha,core}}. \tag{18}$$

η_{He} allows us to write equation (18) in terms of the helium-to-fuel fraction in the core:

$$TBE = \left(\frac{1}{2 \eta_{He} f_{\alpha,core} \Sigma} + 1\right)^{-1}. \tag{19}$$

Equations (10) and (19) highlight a crucial point. TBE can be increased by increasing the helium concentration in the divertor. This can be achieved by increasing the ash concentration in the core at fixed η_{He}. However, the increase in $f_{\alpha,core}$ implies an increase of f_{dil} that decreases the fusion power density. Optimizing tritium usage in the vacuum chamber and keeping high power density are competing goals. Nevertheless, equation (16) shows that TBE can be also improved by increasing the pumping speed ratio Σ.

Equation (16) has another important merit: it allows us to compute the TBE from available experimental measurements. In modern tokamaks (JET Mark IIAP and Mark IIGB divertors [26], Alcator C-mod [28], JT-60U [29]), the helium enrichment fraction has been measured as $\eta_{He} \sim 0.5 - 1$. Assuming $\Sigma = 1, f_{\alpha,core} = 5.5\%$ ($f_{dil} = 5\%$), and $\eta_{He} = 0.1$, one finds the familiar result of TBE = 1%. It is important to note that the TBE increases up to 5%–10% if experimentally measured helium enrichment values ($\eta_{He} = 0.5 - 1$) are considered.

The previous discussion should have clarified the differences between η_f, f_b, and TBE. From a purely mathematical point of view there is no difference in using $\eta_t f_b$ of TBE in a FC model. Nevertheless, the definition of TBE is more suitable to describe the continuous fueling (and exhaust) process in a plasma in equilibrium conditions, and it allows designers to find a tradeoff between FC performance and fusion performance. The implications of equations (10) and (19) are discussed in detail in section 5.2.

1.2. Paper outline

In this work, time-dependent systems-level models of the ARC- and STEP-class FCs are developed in MATLAB Simulink®. The systems-level model provides a suitable tradeoff between model accuracy and computational cost. It enables us to assess the effect of individual design parameters on tritium self-sufficiency and start-up inventory. The results show that tritium self-sufficiency can be achieved in ARC and STEP for a narrow but achievable window of operating parameters: TBE $> 0.5\%$, availability factor (AF) $> 70\%$, DIR fraction $f_{DIR} > 0.3$, and tritium processing time $t_p < 4$ h. A major advantage of ARC versus large FPPs is found in the small size of ARC ($P_{fus} = 525\,MW_{th}$), which translates to a lower start-up inventory.

The paper is organized as follows: section 2 presents the mathematical and computational models for the FC, using the FC for an ARC-class tokamak as reference. Section 3 shows the results from the sensitivity analysis on selected design and operational parameters for the ARC-class tokamak. Section 4 repeats the analysis for two proposed STEP designs, one using an encapsulated breeding blanket (EBB) and the other using a liquid lithium blanket. Section 5 compares ARC results to those from STEP, discusses key topics like the optimal TBE, tritium trapping, and doubling time, and proposes an

R&D path to reduce uncertainties associated with this analysis methodology. Section 6 presents overall conclusions from this analysis.

2. Methodology

2.1. ARC FC layout

CFS's ARC is in a conceptual design phase, and the specific parameters of its FC technologies and components are not finalized. In this paper, it should be understood that when we refer to ARC, we refer to a general 'ARC-class' tokamak, which is characterized by the nominal size and power parameters described in [2], a high-field confinement scheme enabled by high-temperature superconductor magnets [19, 30], and an FLiBe-based LIB for tritium breeding [2, 14, 31]. A high-level layout of the expected FC is shown in figure 1. The FC is divided into two sub-cycles: the outer FC (OFC) and the inner FC (IFC). The OFC encompasses most of the components and subsystems that provide tritium to the IFC. In the ARC-class FPP, the OFC includes the FLiBe LIB and FLiBe coolant channels in the VV[6], the associated tritium extraction systems (TESs), the heat exchanger(s) (HX), and the divertor.

The IFC processes the tritium from the OFC and from the gas stream exhausted by the divertor vacuum pumps, which are considered within the IFC. The IFC supplies the required quantities of deuterium and tritium to the fueling system. Sections 2.1.1 and 2.1.2 provide a detailed description of FC components and subsystems.

2.1.1. OFC. The OFC includes the divertor, FW/VV channels, LIB, TES, and HX(s). It is important to stress that in an ARC-class tokamak, the FLiBe acts as both coolant and tritium carrier. This results in a key distinction between the ARC FC model and the DEMO FC model used in [1]: in ARC, the coolant line and tritium carrier line are part of a single OFC system. There is no coolant purification system (CPS) in the ARC model because the TES fulfills this role in ARC. The layout of ARC FC is shown in figure 1.

Tritium is bred from the ^{6}Li and ^{7}Li in the LIB and in any FLiBe coolant channels located in the VV. The VV channels receive cold ($\sim$800 K) FLiBe directly from the HX [13], where it is heated by the plasma and discharged into the blanket tank (figure 2). Divertor channels are also fed with cold FLiBe from the HX that is discharged into the blanket tank. FLiBe in the blanket tank (which carries tritium) exits via outlet(s) at the top of the tank that is connected to the TES, which extracts tritium from the FLiBe and sends it to the storage and management system. Additional components, such as a tritium permeation membrane, are used on the pathway between the TES and tritium storage to separate tritium from other gases that may be present in the stream exiting the TES (e.g. gases dissolved in FLiBe that may be extracted together with tritium in the TES).

The TES has an efficiency $<$100%, so some fraction of tritium is inevitably carried to the HX by the FLiBe. Generally speaking, the HX is part of the power cycle, not the FC. However, since a small fraction of tritium passes through the HX, the HX must be considered in this FC model. Here we assume that the HX has an active tritium removal system that actively impacts tritium mass transport through the FC. An example is a double-walled HX with sweep gas flowing between the primary and the secondary coolant channels [32]. Tritium that permeates the wall of the primary coolant channel is recovered by the sweep gas and sent to the detritiation system. Any remaining tritium in FLiBe flows back to the LIB, VV channels and divertor channels with the cold FLiBe.

The FC model should also account for unburned tritium ions from the plasma, which act as an additional tritium source in the OFC. Unburned tritium ions can impinge on the plasma-facing surfaces of the divertor and the FW. From there, the tritium ions might diffuse through the structural materials and permeate through the coolant, be trapped in the material, or cycle back into the plasma (note that also the opposite is true: tritium can diffuse from the coolant to the structural materials, depending on its concentration in the two media).

Certain elements of the OFC that are likely to be present in future ARC designs are not modeled here. These include a redox control unit (to monitor and control FLiBe chemistry) and a CPS for the secondary coolant loop (which will inevitably uptake a small amount of tritium from the HX). From a systems-level view, leaving these components out of this iteration of the model should not significantly change results. The redox control unit has no direct FC functions and does not change tritium mass transfer through the FC. The secondary CPS collects tritium that reaches the secondary coolant in the HX and sends it to the detritiation system; this is already accounted for by modeling tritium losses in the HX component and the tritium flow from the HX to the detritiation system.

To summarize, tritium transport in the OFC is mostly dictated by FLiBe flow through the system. Table 1 summarizes the main OFC components.

2.1.2. IFC. The IFC comprises the vacuum pumps and the systems for fuel clean-up, isotope separation, detritiation, tritium storage and management, and fueling. Vacuum pumps pump out tritium from the vacuum chamber, the boundaries of which are defined by the FW and the VV structures (the blanket lies outside the vacuum boundary in an ARC-class tokamak). Unburned tritium is removed from the vacuum chamber by the vacuum pumps. Note that some fraction of the unburned tritium will implant in the plasma facing components; in this model, we assume this fraction is $2{\cdot}10^{-4}$ (equally distributed between FW and divertor), per the value used in

[6] In an ARC-class tokamak, the first wall (FW) and vacuum vessel (VV) are coupled and located inside the breeding blanket. In most conventional designs, the blanket is behind the FW, and the blanket is within the VV boundary. The ARC-class tokamak FW is located on the plasma-facing surface of the inner VV wall [13]. Therefore, in this work, when discussing the ARC-class tokamak, we consider the FW, the VV, and the VV channels as a single component abbreviated as FW/VV.

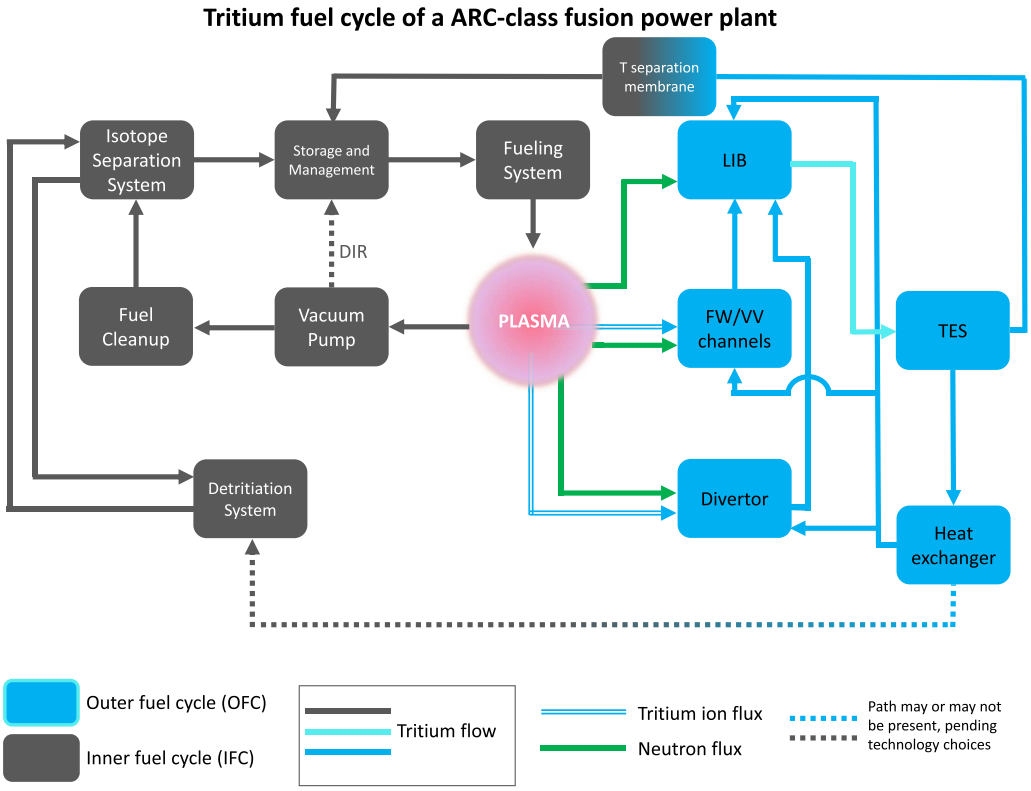

Figure 1. The block diagram shows the high-level fuel cycle of an ARC-class FPP. The outer fuel cycle (OFC) breeds tritium via Li(n), (T) reactions in the blanket and coolant channels. This tritium is passed to the inner fuel cycle (IFC), where it is processed into fuel. Only the components that have been modeled in this work are shown in the figure. The DIR system is represented by a dotted path to indicate that it may or may not be present in the IFC. The dotted path from the heat exchanger to the detritiation system is present if the chosen heat exchanger has an active tritium removal system (e.g. a double-walled heat exchanger with purge gas flow). The inclusion of DIR and the decision to include T extraction in the heat exchanger (HX) are examples of ARC design decisions which have yet to be finalized.

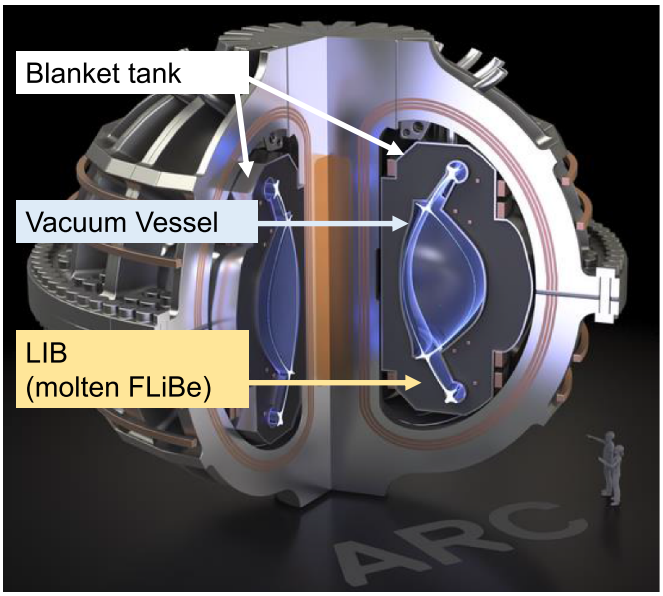

Figure 2. This rendering of an ARC-class tokamak shows the cross-section of the vacuum vessel, liquid immersion blanket, and blanket tank. In contrast to other tokamak FPP concepts, the blanket in an ARC-class plant is outside the vacuum boundary. Rendering of ARC courtesy of Commonwealth Fusion Systems.

Table 1. Key components in the outer fuel cycle of a DT-burning fusion power plant, along with a non-comprehensive list of examples.

Component	Description	Examples
Blanket (LIB)	The blanket employs a lithium-containing material (FLiBe in the LIB), which interacts with neutrons from the D-T reactions in the plasma to produce tritium.	LIB (ARC) [2], helium-cooled lithium lead (DEMO) [40], water-cooled lithium lead (DEMO) [40], helium-cooled pebble bed (DEMO), dual-coolant lithium lead (DEMO) [40], liquid lithium (STEP).
First wall and vacuum vessel (FW/VV)	The FW surrounds the plasma. It must withstand high heat loads ($\sim$MW m^{-2}) and damaging PMI. It is usually made of high-Z materials. In ARC, the FW is immediately adjacent to the VV, which is inside the blanket.	Tungsten FW (ARC, expected), Be FW (JET-ILW [41]) VV: TBD, but low-activation material likely necessary.
Divertor	The divertor provides ash removal and heat extraction. The divertor design depends on the plasma magnetic configuration. It must withstand very high heat loads ($\sim$10 MW m^{-2}) and strong particle bombardment.	Tungsten divertor (ARC, expected [13]), ITER tungsten cassette assemblies. Single null [42], double null [43], snowflake [44].
Heat exchanger (HX)	The HX transfers thermal energy from the primary coolant to the secondary coolant.	Shell and tube heat exchanger [45], plate heat exchanger, concentric pipe heat exchanger [46], heat pipes [47].
Tritium extraction system (TES)	The TES removes tritium from the tritium carrier (which may be solid, liquid, or gas depending on design). The extracted tritium is sent to the inner fuel cycle.	Permeator against vacuum [48–50], liquid–liquid contractor [51], gas-bubble columns [52], vacuum sieve tray [53].

[1][7]. The vast majority of tritium fuel passes through the IFC, so its dynamics have a critical impact on the performance of the overall FC.

The exhaust gas from the vacuum pumps is processed in the fuel clean-up system that separates hydrogenic species from plasma enhancement gases (Ar, Ne, and other inert gases) and He ashes. If the DIR line is implemented [25] (see table A.12 in the appendix for the mathematical implementation in the model), a metal foil pump (MFP) [38] or a multi-stage cryopump will be located upstream of the fuel clean-up to provide a preliminary separation of hydrogenic species from the exhaust gas. Separation of hydrogenic species from the exhaust gas by the DIR reduces processing burdens on the fuel clean-up system and isotope separation system (ISS), speeding up the IFC dynamics and reducing the tritium inventories in the IFC components. The DIR concept was originally proposed by Day and Giegerich [25] and Giegerich and Day [39] for the DEMO FC. It features an MFP (or a multi-stage cryopump) that can separate a large fraction of hydrogenic species from the exhaust gas (up to 90% [25]), and two identical pumping trains exploiting a linear diffusion pump and a liquid ring pump. The first train pumps the pure fuel permeated through the MFP directly to the storage and management system, whereas the second train pumps the remaining exhaust gas to the fuel clean-up system. Downstream of the fuel clean-up, the ISS separates hydrogen from deuterium and tritium. The separated deuterium and tritium are sent to the storage and management system. The ISS also processes tritium coming from the TES and from the detritiation system. We refer to a general 'black box' detritiation system without considering specific engineering details in this work.

The storage system fulfills many functions. First, it contains the start-up tritium inventory required to start FPP operations. The start-up inventory will be on the order of kilograms, so an effective storage system is critical to plant safety. Second, it works as a short-term buffer for fresh fuel. Lastly, it provides long term storage for the tritium that will be eventually transferred to new fusion power plants for start-up. The last major IFC component is the fueling system, which injects fresh fuel in the vacuum chamber. Table 2 summarizes the key IFC components.

2.2. FC model

2.2.1. Mathematical formulation. The FC model in this work is based on the **resident time method (RTM)** proposed in [70] and exploited in the recent analysis of the DEMO FC [1]. In the RTM, a lumped model is used to describe each component of the FC. The tritium balance for each component is described with a time-dependent, ordinary differential equation (ODE):

$$\frac{\mathrm{d}I_i}{\mathrm{d}t} = \sum_{j\neq i}\left(f_{j\to i}\frac{I_j}{\tau_j}\right) - (1+\epsilon_i)\left(\frac{I_i}{\tau_i}\right) - \lambda I_i + S_i \qquad (20)$$

with initial conditions described by equations (21) and (22):

$$I_i(t=0) = 0, \forall i \neq \text{storage} \qquad (21)$$

$$I_{\text{storage}}(t=0) = I_{\text{startup}}. \qquad (22)$$

[7] Tritium implantation in PFCs is just one of the many phenomena involved in plasma material interactions (PMIs). Modeling of PMI requires a tremendous effort due to the complex physical and chemical mechanisms involved and the multiscale nature of the problem [33]. The fraction of unburned tritium that implants in the PFC is usually quantified by surface analysis of small material samples from ion irradiation setups [34] or experimental devices (e.g. JET-ILW [35], JT-60U [36], ASDEX Upgrade [37], etc). No experimental data is available for the ion fluxes and energies expected in fusion devices like ARC-class FPPs or STEP-class FPPs. Therefore, we assumed a tritium implantation fraction of $2{\cdot}10^{-4}$ for consistency with the analysis from [1].

Table 2. Key IFC components and a non-exhaustive list of associated technologies.

Component	Description	Examples
Vacuum pump	Vacuum pumps provide exhaust pumping from the vacuum chamber. The exhaust contains unburned fuel, He ashes, and plasma enhancement gases.	Cryopumps [54], vapor diffusion pumps [55], liquid ring pumps [56].
Fuel clean-up	Fuel clean-up separates hydrogenic species from the other exhaust gases (plasma enhancement gases, helium ash).	Pd-Ag alloy permeator [57].
Isotope separation system (ISS)	ISS separates hydrogen, deuterium, and tritium.	Pressure swing absorption [58], thermal diffusion [59], cryogenic distillation [60], thermal cycling absorption process [61].
Detritiation system	The detritiation system removes tritium in trace amount from water (water detritiation system) and exhaust (exhaust detritiation system).	Wet scrubber [62], combined electrolysis and catalytic exchange (CECE) process [63, 64].
Storage and management system	The storage and management system is used to store the initial tritium inventory and the tritium that eventually will be transferred to new FPP.	Uranium beds [65], ZrCo beds [66], LaNi beds [67, 68].
Fueling system	The fueling system delivers the required fuel mixture to the plasma.	Gas gun pellet injection [69], centrifuge pellet injection [69].
DIR loop	The DIR loop separates hydrogenic species from the gas exhaust by exploiting hydrogen superpermeation through metal foils (for MFP) or hydrogen cryosorption in different pump chambers (for cryopumps).	Possible DIR technologies include MFP or a multi-stage cryopump, linear diffusion pumping, and liquid ring pumping [39]

Subscripts i and j refer to the generic ith and jth component, I is tritium inventory, τ is tritium residence time, λ is the tritium decay rate, and ϵ is the fraction of tritium lost due to non-radioactive phenomena (e.g. leakages). The evolution of the tritium inventory in the ith component, I_i, depends on:

- Tritium flows entering component i from the jth components connected to i, $\sum_{j\neq i}\left(f_{j\rightarrow i}\frac{I_j}{\tau_j}\right)$
- Outflow from component i, $\frac{I_i}{\tau_i}$
- Non-radioactive and radioactive tritium losses, $\epsilon_i\frac{I_i}{\tau_i}-\lambda I_i$
- Tritium generation in component i, S_i.

Specifically, ϵ_i is the tritium residence time in component i, ϵ_i is the non-radioactive tritium loss fraction in component i, and $f_{j\rightarrow i}$ is a multiplying factor representing the fraction of component j's outflow that is directed toward component i. If component j has only one output, to component i, then $f_{j\rightarrow i}=1$. I_{storage} is the tritium inventory in the storage system, and I_{startup} is the start-up inventory (see section 2.2.2 for additional details on these inventories).

The key advantages of the RTM are its computational speed, design flexibility, and the ability to model tritium flow through a component using simple parameters without needing engineering details. For a target condition, such as tritium self-sufficiency, the RTM can be used to understand the required performance from each component, such as blanket TBR, providing researchers with meaningful design targets.

The physical and chemical processes underlying tritium transport in FLiBe are not well understood, and there is a wide spread in available experimental data [71]. As of 2022, there are multiple new experimental efforts underway in the United States to understand FLiBe chemistry, motivated by fusion applications like the ARC LIB and fission applications like the molten salt reactor under development by Kairos power. However, until the data from these projects is available, we must rely on coarse high-level models like the RTM. Furthermore, as pointed out in [1], the time and length scales that describe the FPP FC are not suitable for an atomic-scale simulation of tritium transport. Instead, each component is a black box characterized by tritium residence time within the component and component-specific parameters (e.g. tritium extraction efficiency for the TES, or DIR fraction for DIR). Eventually, new experimental data will be used to reduce uncertainty on the value of these parameters [31].

FPP operations are expected to be intermittent, and are modeled by the AF[8]. The AF accounts for both pulsed operations and possible outages due to system failure. Equation (23) defines AF,

$$AF=\frac{t_{\text{on}}}{t_{\text{on}}+t_{\text{off}}} \tag{23}$$

where t_{on} is the pulse duration and t_{off} is the downtime between two consecutive pulses. The AF is an effective way to consider FPP downtime in the RTM. It is important to note that the definition of AF in this context considers the FC as unavailable whenever tritium is not produced during operations. This

[8] We use the term 'availability factor' for consistency with the analysis carried out in [1]. However, AF has a slightly different meaning here (fraction of time during which the FPP can effectively breed tritium) than it does in its reliability engineering definition (fraction of time during which the FPP is operating).

definition stems from our focus on assessing the system capability to breed tritium, which is the critical function in a tritium self-sufficiency analysis. Consequently, this definition is slightly more stringent compared to the one used in reliability engineering [1]:

$$\mathrm{AF_{rel}} = \frac{\mathrm{MTBF}}{\mathrm{MTBF} + \mathrm{MTTR}}. \tag{24}$$

In equation (24), MTBF represents the mean time between failures, and MTTR stands for mean time to repair. In an ideal scenario where no failures occur (i.e. $\mathrm{MTBF} \to \infty$), $\mathrm{AF_{rel}} = 1$. However, for our purposes, AF may be less than 1 because it considers the system unavailable even when it operates correctly but does not breed tritium (e.g. during the dwell time).

The RTM is not the only option for studying the FPP FC, and it is worthwhile to briefly consider the advantages and drawbacks of other approaches. More advanced models have been developed that include detailed component simulations within a dynamic model [72, 73]. However, a detailed design of FC components is required to implement these models, and they are computationally expensive, as a full component-level simulation is run at every time step. Another notable FC modeling effort is found in [74], which details a lumped model of the tritium FC for the EU-DEMO FPP and leverages the preliminary design parameters available for the EU-DEMO FC. Their model computes the tritium mass flow rates exchanged between the components without explicitly accounting for the residence time. FPP operations in [74] are described by sampling failure and outage times from a log-normal distribution instead of using a mean AF. This accounts for the wide range of timescales that will characterize FPP outage times, from minutes (e.g. fixing a stuck valve) to days (e.g. divertor cassette failure) and captures a more realistic system evolution, albeit at the expense of higher computational costs. We implement a mean AF in our approach because design uncertainties for the ARC and STEP FCs outweigh the benefits of the more detailed AF approach in [74]. The lumped model from [74] also uses the expected achievable TBR in EU-DEMO as a model input that can vary narrowly around the nominal value. Doubling time is then a model output in [74]. This is a reasonable approach when achievable the TBR is known and few major design changes to the FPP are expected. However, ARC and STEP are in an early design stage, and it is more useful to set a desired doubling time as an input parameter for the RTM model and then calculate the TBR that will be required to achieve it.

2.2.2. Start-up inventory and reserve inventory. The overall tritium inventory within the FPP site boundary is relevant to safety and regulation. The RTM model is most concerned with the reserve inventory (I_{res}) and the start-up inventory (I_{startup}). Both are key to plant self-sufficiency, and both are major contributors to the overall tritium inventory at the plant. An optimized FC will minimize I_{res} and I_{startup} (for the purposes of better safety and smaller regulatory burdens) without sacrificing tritium self-sufficiency.

Equation (25) gives I_{res}, the amount of tritium required to keep the reactor fueled and operating for a prescribed reserve time (t_{res}) if a fraction q of the FC fails:

$$I_{\mathrm{res}} = \frac{\dot{N}_{\mathrm{T,burn}}}{\mathrm{TBE}} q t_{\mathrm{res}}. \tag{25}$$

The reserve time can be chosen according to economic, safety, and reliability considerations. In theory, it can be equal to zero. Robust and reliable FPPs will not require large I_{res}, which in turn eases safety and regulatory burdens by decreasing overall site inventory.

I_{startup} is the amount of tritium required in fuel storage at the beginning of operations to start and initially run the plant. At the beginning of operations, the tritium bred in the blanket is not readily available as fuel: tritium will build up in components to a certain equilibrium level, plus it takes time for tritium to pass through the FC systems. Hence, the tritium for FPP fueling is initially provided by the storage system. Furthermore, the start-up inventory must also compensate for the non-radioactive and radioactive tritium losses from the FC components. Initially, the storage inventory decreases as tritium is used for fuel, is recirculated, or is lost. As bred tritium becomes available, the storage inventory begins to increase. The minimum storage inventory is an inflection point, and it occurs at the inflection time t_{infl}, which is on the order of the total residence time in the OFC plus the residence time in the ISS (i.e. the time needed to make newly bred tritium available as fuel).

In a ideal optimized FC model, the storage inventory reaches a minimum value of zero (temporarily) at the inflection point, indicating that the start-up inventory at $t = 0$ was minimized ($I_{\mathrm{startup,opt}}$) without sacrificing tritium self-sufficiency. For $I_{\mathrm{startup}} < I_{\mathrm{startup,opt}}$, tritium self-sufficiency cannot be achieved, and the FPP will run out of tritium before it can be sustained on bred tritium alone. However, due to uncertainties and possible failures in the FC systems, a real FPP will have a reserve inventory for the first days of operation. In this case, the storage inventory reaches a minimum value equal to the reserve inventory. The start-up inventory necessarily increases by an amount equal to I_{res}. Figure 3 shows I_{storage} as a function of time for an ideal and realistic FPP.

2.2.3. Dynamics of a basic FC model. In this subsection we describe the dynamics of a basic FC to provide a common background to the readers. An analytical solution can be indeed found for very simple FC models, while this task becomes overwhelming for more complex models such as the ones developed for ARC- and STEP-class tokamaks in the next sections.

Figure 4 shows a simple FC model where all IFC components except the storage system are collapsed in a single 'IFC' block, and all the OFC components are collapsed in a single 'OFC' block. The storage system is represented its own block so that we can explicitly track inventory buildup. The fueling system is neglected for simplicity. We assume a set of reasonable parameters: $\dot{N}_{\mathrm{T,burn}} = 9 \cdot 10^{-7}\,\mathrm{kg\,s^{-1}}$, $\mathrm{TBE} = 1\%$, $\mathrm{TBR} = 1.08$, $I_{\mathrm{startup}} = 1.5\,\mathrm{kg}$ $\tau_{\mathrm{IFC}} = 4\,\mathrm{h}$ and

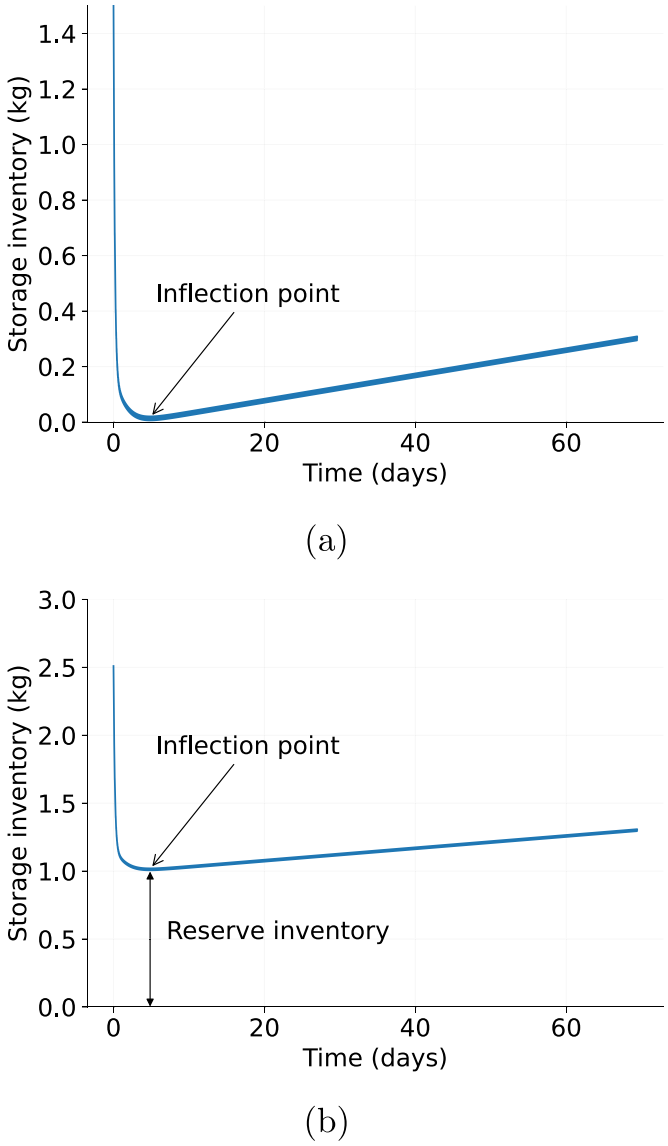

Figure 3. Evolution of the storage inventory during plant operations. (*a*) Ideal scenario (AF = 1) with no reserve inventory. The minimum storage inventory is zero at the inflection point. (*b*) Realistic scenario (AF < 1) with a reserve inventory of 1 kg. The minimum storage inventory equals the reserve inventory at the inflection point. I_{storage} decreases from $t = 0$ to $t = t_{\text{infl}}$ because the bred tritium is not immediately available as fuel. The inflection point is reached when the tritium bred at $t = 0$ has passed through the OFC, the ISS, and reached the storage system. For $t > t_{\text{infl}}$ the storage inventory increases linearly due to the constant inflow of bred tritium (assuming no interruption to plant operation). The values reported in the plots do not refer to any particular design, and were chosen to emphasize the contribution of the reserve inventory to the storage inventory.

$\tau_{\text{OFC}} = 24$ h. Radioactive and non-radioactive tritium losses are neglected.

The storage system provides a constant tritium flow for fueling equal to $\frac{\dot{N}_{\text{T,burn}}}{\text{TBE}}$. The tritium production in the OFC is equal to $\dot{N}_{\text{T,burn}} \cdot \text{TBR}$, while the unburned tritium is exhausted from the vacuum chamber at a rate equal to $\dot{N}_{\text{T,burn}} \frac{1-\text{TBE}}{\text{TBE}}$. The characteristic timescales of the IFC and OFC are defined by their tritium residence times, τ_{IFC} and τ_{OFC}. Equations (26)–(30) describe the evolution of the tritium inventories in the basic FC

$$\frac{\mathrm{d}I_{\text{OFC}}(t)}{\mathrm{d}t} = \dot{N}_{\text{T,burn}} \cdot \text{TBR} - \frac{I_{\text{OFC}}(t)}{\tau_{\text{OFC}}} \tag{26}$$

$$\frac{\mathrm{d}I_{\text{IFC}}(t)}{\mathrm{d}t} = \frac{1-\text{TBE}}{\text{TBE}}\dot{N}_{\text{T,burn}} + \frac{I_{\text{OFC}}(t)}{\tau_{\text{OFC}}} - \frac{I_{\text{IFC}}(t)}{\tau_{\text{IFC}}} \tag{27}$$

$$\frac{\mathrm{d}I_{\text{storage}}(t)}{\mathrm{d}t} = \frac{I_{\text{IFC}}(t)}{\tau_{\text{IFC}}} - \frac{\dot{N}_{\text{T,burn}}}{\text{TBE}} \tag{28}$$

with initial conditions:

$$I_{\text{IFC}}(0) = I_{\text{OFC}}(0) = 0 \tag{29}$$

$$I_{\text{storage}}(0) = I_{\text{startup}} \tag{30}$$

where I_{IFC}, I_{OFC}, and I_{storage} are the tritium inventories in the IFC, OFC and storage system, respectively. The analytical solution of the system of equations defined by equations (26)–(30) is reported in equations (31)–(33).

$$I_{\text{OFC}}(t) = \dot{N}_{\text{T,burn}}\tau_{\text{OFC}}\text{TBR}(1 - \mathrm{e}^{-t/\tau_{\text{OFC}}}) \tag{31}$$

$$\begin{aligned} I_{\text{IFC}}(t) = {} & \dot{N}_{\text{T,burn}}\tau_{\text{IFC}}\frac{1-\text{TBE}}{\text{TBE}}(1 - \mathrm{e}^{-t/\tau_{\text{IFC}}}) \\ & + \dot{N}_{\text{T,burn}}\ \text{TBR}\ \tau_{\text{IFC}}(1 - \mathrm{e}^{-t/\tau_{\text{IFC}}}) \\ & + \dot{N}_{\text{T,burn}}\ \text{TBR}\ \frac{\tau_{\text{IFC}}\tau_{\text{OFC}}}{\tau_{\text{OFC}} - \tau_{\text{IFC}}}(\mathrm{e}^{-t/\tau_{\text{IFC}}} - \mathrm{e}^{-t/\tau_{\text{OFC}}}) \end{aligned} \tag{32}$$

$$\begin{aligned} I_{\text{storage}}(t) = {} & I_{\text{startup}} + \dot{N}_{\text{T,burn}}(\text{TBR} - 1)t \\ & + \dot{N}_{\text{T,burn}}\ \text{TBR}\ \frac{{\tau_{\text{IFC}}}^2}{\tau_{\text{OFC}} - \tau_{\text{IFC}}}(1 - \mathrm{e}^{-t/\tau_{\text{IFC}}}) \\ & + \dot{N}_{\text{T,burn}}\ \text{TBR}\ \frac{{\tau_{\text{OFC}}}^2}{\tau_{\text{OFC}} - \tau_{\text{IFC}}}(1 - \mathrm{e}^{-t/\tau_{\text{OFC}}}) \\ & - \dot{N}_{\text{T,burn}}\tau_{\text{IFC}}\frac{1-\text{TBE}}{\text{TBE}}(1 - \mathrm{e}^{-t/\tau_{\text{IFC}}}). \end{aligned} \tag{33}$$

Equations (32) and (33) highlight a crucial feature of the FC dynamics for TBE < 1. The FPP burns only a fraction of the tritium injected in the vacuum chamber, and the net tritium flow through the storage system is approximately $-\frac{\dot{N}_{\text{T,burn}}}{\text{TBE}}$ during the initial transient. It should be noted that the unburned tritium flow ($\dot{N}_{\text{T,burn}}\frac{1-\text{TBE}}{\text{TBE}}$) takes $\sim\tau_{\text{IFC}}$ to be processed and to flow back to the storage system. Furthermore, the contribution of the unburned tritium flow to the total tritium flowing in the storage system is dominant (at steady state) if TBE $\ll 1$. Since $I_{\text{IFC}}(t)$ does not reach its steady-state value until $t \sim 3\tau_{\text{IFC}}$[9], a large fraction of I_{startup} is used to keep the FPP operating during the initial transient. I_{storage} reaches t_{infl} at $t \sim 3\tau_{\text{OFC}}$ (i.e. when the tritium bred in the OFC reaches the storage system) and thereafter begins to increase. The exact inflection time can be

[9] We recall that solutions to ODE in the form $(1 - \mathrm{e}^{-\frac{t}{\tau}})$ reach the steady state value in $t \sim 3\tau$, as $(1 - \mathrm{e}^{-\frac{3\tau}{\tau}}) \sim 0.95$

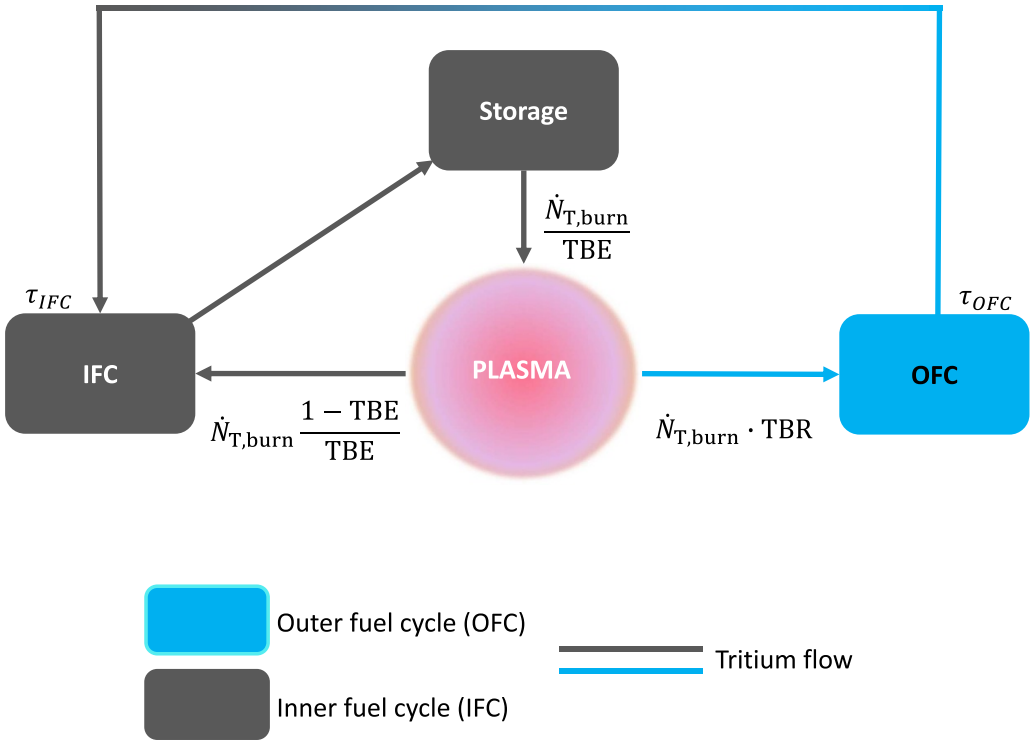

Figure 4. A basic fuel cycle layout. All IFC components except the storage system are collapsed in a single block with residence time τ_{IFC}. Similarly, all the components in the OFC are collapsed in a single block with residence time τ_{OFC}. The tritium flows exchanged by the systems are depicted by the arrows.

computed analytically by setting the time derivative of I_{storage} equal to zero and solving for t:

$$\left.\frac{\mathrm{d}I_{\mathrm{storage}}}{\mathrm{d}t}\right|_{t=t_{\mathrm{infl}}} = 0 \tag{34}$$

that gives $t_{\mathrm{infl}} = 2.7$ days, which is approximately $3\tau_{\mathrm{OFC}}$.

The steady-state value of the tritium mass flow rate into the storage system is equal to:

$$\dot{m}_{\mathrm{in,storage,ss}} = \dot{N}_{\mathrm{T,burn}}\mathrm{TBR} + \dot{N}_{\mathrm{T,burn}}\frac{(1-\mathrm{TBE})}{\mathrm{TBE}} \tag{35}$$

which is larger than the tritium flow exiting the storage system:

$$\dot{m}_{\mathrm{out,storage}} = -\frac{\dot{N}_{\mathrm{T,burn}}}{\mathrm{TBE}} \tag{36}$$

as expected from the fact that $\mathrm{TBR} > 1$.

2.2.4. Computational model. The MATLAB Simulink® model of the ARC FC is based on the layout shown in figure 1. The differential equations used to model each component are given in the appendix, and so only a brief overview of the model is provided here. Equation (20) is the key equation used to describe each component. The only component that was not modeled is the fueling system. Instead, an outflux equal to the tritium fueling rate is added to the equation describing the storage and management system (see equation (A.11) in the appendix for additional details). Pulsed operation was modeled using a pulse source[10] for the tritium generation in the blanket and channels, for the tritium implanted into the FW and the divertor, and for the tritium exhausted by the vacuum pumps. The pulse width is equal to AF[11].

The computation of a suitable TBR and start-up inventory requires an iterative approach. Both the TBR and I_{startup} are unknown at the beginning of the simulation. We stress that the TBR value returned by the simulation is the $\mathrm{TBR_r}$, where $\mathrm{TBR_r}$ is the minimum TBR required for the plant to achieve tritium self-sufficiency and double I_{startup} in the prescribed doubling time t_{d}. While I_{startup} is mostly insensitive to $\mathrm{TBR_r}$, the opposite is not true. If I_{startup} increases and the prescribed doubling time remains the same, the TBR must increase. At each iteration, $(I_{\mathrm{storage}}(t) - I_{\mathrm{res}})$ is computed and the start-up inventory is updated accordingly. The TBR is gradually increased, and simulations are run until two constraints are satisfied:

$$I_{\mathrm{storage}}(t) - I_{\mathrm{res}} > 0, \forall t \geqslant 0 \tag{37}$$

[10] A pulse source (or pulse generator) in Matlab Simulink® generates a square wave signal of any real variable. The pulse source is characterized by four parameters: amplitude (A), pulse width (% of period) (w), period (T) and phase delay (ϕ). In our model $A = \mathrm{TBR} \cdot \dot{N}_{\mathrm{T,burn}}$, $w = \mathrm{AF}$, $T = (t_{\mathrm{on}})$, and $\phi = 0$.

[11] Note that by using AF all the pulses have an effective duration of $\mathrm{AF} \cdot t_{\mathrm{on}}$. This clearly differs from a real case scenario, where the pulse duration is t_{on}, but some of the pulses are missed due to system failures. The averaging procedure introduced by AF changes the dynamics of the system on a short time scale (i.e. hours), but no impacts on the results are expected on longer time scales (i.e. years).

$$I_{\text{storage}}(t = t_{\text{d}}) = 2I_{\text{startup}}. \tag{38}$$

The first constraint, equation (37), requires that at any time during operation, the desired reserve inventory I_{res} is available in tritium storage. The second constraint, equation (38), requires that the desired t_{d} is achieved by the FPP.

There is sometimes minor confusion about the precise definition of 'doubling time.' In this work, we define t_{d} as the time needed to store an amount of tritium equivalent to $2I_{\text{startup}}$. However, t_{d} is sometimes defined as the time required to breed the minimum amount of tritium needed to start a second, identical FPP without sacrificing the tritium self-sufficiency of the first FPP:

$$I_{\text{storage}}(t = t_{\text{d}}) = I_{\text{startup}} + I_{\text{res}}. \tag{39}$$

In this work, we use the more straightforward definition given in equation (38). However, it is useful to remember that $I_{\text{storage}}(t_{\text{d}})$ can be very different for each definition.

An advantage of MATLAB Simulink® is that it automatically selects the (variable) stepsize and the numerical solver (that implements the adaptive step size) for the system of equations at each point in the model. This is important because the timescales involved in the fusion FC (FPP lifetimes are given in decades) are much larger than the required stepsize at the beginning of the simulation (10–1000 s). Once the tritium inventory of all components (other than tritium storage) have reached quasi-steady state, the timestep is increased for the sake of computational efficiency. The scripts and the models to reproduce the results are available on GitHub [75].

3. Tritium self-sufficiency in an ARC-class fusion power plant

In this section, we use the methods described in section 2 to analyze the FC of an ARC-class FPP and determine the conditions needed to achieve tritium self-sufficiency. Section 3.1 introduces the model parameters. Section 3.2 reports the one-at-a-time sensitivity analysis [76]. Results in sections 3.1 and 3.2 are normalized with respect to the mean value to better show how TBR_{r} and I_{startup} depend on the design parameters. Sections 3.3–3.9 present the quantitative dependencies of TBR_{r} and I_{startup} on individual design parameters. Section 3.10 describes three example design and operational scenarios for tritium self-sufficient ARC-class FPPs.

3.1. ARC-class tokamak model parameters

Here, we choose a reference configuration for ARC and vary the design parameters to understand the sensitivity of TBR_{r} and I_{startup} to different design choices. This is a simple but effective way to perform sensitivity analysis, also known as one-at-a-time sensitivity analysis [76]. Table 3 lists the design parameters for the baseline ARC case and the range of values considered in the sensitivity analysis. Results presented in section 3 reference these values unless otherwise specified. The baseline case considers a 525 MW_{th} ARC-class tokamak with an availability factor >50%, a low DIR fraction ($f_{\text{DIR}} = 0.3$), a 4 h tritium processing time (time for tritium to be processed in the fuel clean-up system and ISS), the ability to operate on tritium fuel reserves for up to 24 h, and an aggressive target for t_{d} (2 yr, in contrast to the 5–10 yr expected for DEMO-class FPPs [74]).

A preliminary analysis suggests that TBE = 1%–3% for ARC [77]. The non-radioactive loss fraction is set to 10^{-4} as in [1]. However, the reader should be aware that the non-radioactive loss fraction significantly affects the results of the FC analysis and TBR_{r} (see figure A.24 in the appendix). An availability factor lower than 50% is not considered, as commercial electricity generating plant designs with AF < 50% will not be commercially viable[12]. The tritium processing time t_{p} ranges from 1 h to 12 h. Abdou *et al* [80] assumed a tritium processing time in the range 1–24 h based on the experience from the tritium systems test assembly (TSTA) experiment [81], which reported $t_{\text{p}} = 24$ h. The same author restricted the range to 1–12 h in the more recent work on tritium FC analysis [1]. A recent analysis for DEMO FC assumed $t_{\text{p}} = 4800$ s [25]. Coleman *et al* [74] performed FC analyses considering a $t_{\text{p}} = 5 \pm 2$ h. The range 1 h to 12 h is therefore considered suitable to investigate a wide range of possible operating scenarios. The reader should be aware that t_{p} here is considered to be the sum of the fuel clean-up time τ_{fc} and the ISS residence time τ_{ISS} only. We kept this definition of t_{p} for consistency with the work from [1]. An alternative definition of t_{p} for an FPP with DIR technology can be easily derived from a tritium mass balance in the DIR loop, fuel cleanup system and ISS:

$$I_{\text{tot}} = I_{\text{DIR}} + I_{\text{fc}} + I_{\text{ISS}} \tag{40}$$

where I_{tot} is the total mass of tritium in the control volume encompassing the DIR loop, fuel cleanup system and ISS. Recalling that $\dot{m}_i = \frac{I_i}{\tau_i}$ (section 2.2.1), equation (40) can be written as:

$$\dot{m}_{\text{tot}} t_{\text{p,eff}} = \dot{m}_{\text{DIR}} \tau_{\text{DIR}} + \dot{m}_{\text{fc}} \tau_{\text{fc}} + \dot{m}_{\text{ISS}} \tau_{\text{ISS}} \tag{41}$$

where $\dot{m}_{\text{tot}} = \dot{m}_{\text{DIR}} + \dot{m}_{\text{fc}} + \dot{m}_{\text{ISS}}$, and we have defined the effective (or average) tritium processing time ($t_{\text{p,eff}}$) as the average time required by the tritium to flow from the vacuum pumps to the storage system (passing through the DIR or through the fuel cleanup and ISSs). Since $f_{\text{DIR}} \equiv \frac{\dot{m}_{\text{DIR}}}{\dot{m}_{\text{tot}}}$, equation (41) can be rewritten as:

$$t_{\text{p,eff}} = \tau_{\text{DIR}} f_{\text{DIR}} + (1 - f_{\text{DIR}})(\tau_{\text{ISS}} + \tau_{\text{fc}}). \tag{42}$$

[12] A simple calculation can show why AF < 50% is not commercially viable. The payback time (PT) of a FPP can be computed to a first approximation as $\text{PT} = C_{\text{tot}}/(8760 P_{el} \text{AF} c_{el})$, where PT [y] is the payback time, C_{tot} [$] is the total FPP cost (here assumed equal to the overnight cost for sake of simplicity), and c_{el} [$\$\,\text{kW}\,\text{h}^{-1}$] is the electricity cost. For FPPs, C_{tot} is still unknown, but a reasonable value can be extrapolated from innovative nuclear reactor designs, such as GEN-IV molten salt reactors (MSR). The overnight cost of an MSR ranges from $1B to $10B [78]. Assuming $C_{\text{tot}} = \$5\text{B}$ and $c_{el} = 0.129\,\$\,\text{kW}\,\text{h}^{-1}$ (the average price of U.S. electricity in June 2022 [79]), for $P_{el} = 200\,\text{MW}_e$ (the ARC-class tokamak power output) and AF = 0.5, the resulting payback time is PT = 44 yr, which is too long to make the FPP economically attractive.

Table 3. Design parameters for the baseline ARC-class FPP fuel cycle analyzed in section 3.

Parameter	Symbol	Value	Range	Units
Fusion power	P_{fus}	525	—	MW_{th}
Tritium burn rate	$\dot{N}_{\text{T,burn}}$	$9.3{\cdot}10^{-7}$	—	kg s^{-1}
Pulse duration	t_{pulse}	1800	1800–3600	s
Time between pulses	t_{off}	60	60–120	s
Tritium burn efficiency	TBE	0.02	0.005–0.1	—
Non-radioactive loss fraction	ϵ_i	10^{-4}	—	—
Availability factor	AF	0.7	0.5–1	—
Tritium processing time	t_{p}	4	1–12	h
Doubling time	t_{d}	2	—	y
Fraction of the system failing	q	0.25	—	—
Reserve time	t_{res}	24	0–48	h
Direct internal recycling fraction	f_{DIR}	0.3	0.1–0.9	—

Table 4. Tritium residence time in the fuel cycle components and systems. Nominal value for the baseline case and the range used in the parametric analysis are reported.

Component	Symbol	Value	Range	Units
Breeding zone	τ_{BZ}	1.25	1–240	h
First wall	τ_{FW}	1000	—	s
Divertor	τ_{div}	1000	—	s
Tritium extraction system	τ_{TES}	24	1–240	h
Heat exchanger	τ_{HX}	1000	—	s
Vacuum pump	τ_{vp}	600	—	s
Fuel clean-up	τ_{fc}	0.3	0.1–1	h
Isotope separation system	τ_{ISS}	3.7	0.9–11	h
Detritiation system	τ_{det}	1	—	h

This definition is useful when one wants to investigate the effect of DIR at a very high level, without entering into system-level details. Since our model is system-level and allows for a more detailed treatment we do not use this definition. Hence, the value of t_{p} is independent of f_{DIR} in this work. t_{res} ranges from 1 to 48 h. Larger values of t_{res} leads to impractical start-up inventories, as shown in section 3.8.

The second set of relevant parameters for the model are the tritium residence times in individual FC components and systems. These values are reported in table 4. Note that we refer to a general 'breeding zone' and not to the LIB, because tritium will be produced in FLiBe-containing VV and divertor channels. The residence time in the breeding zone was quantified from the steady-state tritium inventory computed by Ferrero *et al* [14]. FC simulations with the present model were run for different τ_{BZ} until the breeding zone tritium inventory reached 3 g, which was the value found in [14]. This resulted in a $\tau_{\text{BZ}} = 1.25$ h. The fuel clean-up and ISS residence time sum to 4 h for the baseline case, 1 h for a short processing time case, and 12 h for a long processing time case [1]. The storage residence time does not appear in table 4 because the tritium outflow from the tritium storage system is defined by the required fueling rate.

3.2. Sensitivity analysis

The following eight parameters have been varied for the sensitivity analysis: AF, TBE, DIR fraction (f_{DIR}), breeding zone residence time (τ_{FW}), TES efficiency (η_{TES}), tritium processing time (t_{p}), reserve time (t_{res}) and doubling time (t_{d}). During each simulation, all but one of the parameters are fixed. The parameter being studied is varied through the range specified in table 5. The mean values and the range specified in table 5 are slightly different from the nominal values specified in tables 3 and 4 to better emphasize the sensitivities of TBR_{r} and I_{startup}.

Figure 5 shows the results from the sensitivity analysis for TBR_{r}. The sensitivity index coefficient (IC) was computed as:

$$\text{IC} = \frac{\Delta Y}{\Delta X}\frac{X_{\text{mean}}}{Y_{\text{mean}}} \tag{43}$$

where ΔY is the change in TBR_{r} or I_{startup} due to a change of ΔX in one of the design parameters. ΔX is computed as:

$$\Delta X = x_{\text{max}} - x_{\text{min}} \tag{44}$$

where $x_{\text{max}} = \mu + \sigma$ and $x_{\text{min}} = \mu - \sigma$, μ is the mean value and σ is half of the range of variation. The relative sensitivity index coefficient (RIC) makes it easier to understand the dependence of TBR_{r} and I_{startup} on the design parameters. It is plotted in figure 5 and is given by:

$$\text{RIC} = \frac{\text{IC}_i}{\sum_{n}^{N_{\text{params}}} \text{IC}_n} \tag{45}$$

Table 5. Mean value μ and range σ of the parameters used in the section 3.2 sensitivity analysis. Each parameter was varied across the specified range, centered on the mean value, in increments of (range)/6.

Parameter	Symbol	Mean value	Range	Units
Availability factor	AF	0.75	±0.25	—
Tritium burn efficiency	TBE	2.5	±2.5	%
DIR fraction	f_{DIR}	0.5	±0.5	—
Breeding zone residence time	τ_{BZ}	13	±11	h
TES efficiency	η_{TES}	0.7	±0.3	—
Tritium processing time	t_{p}	6.5	±5.5	h
Reserve time	t_{res}	24	±24	h
Doubling time	t_{d}	6	±5	y

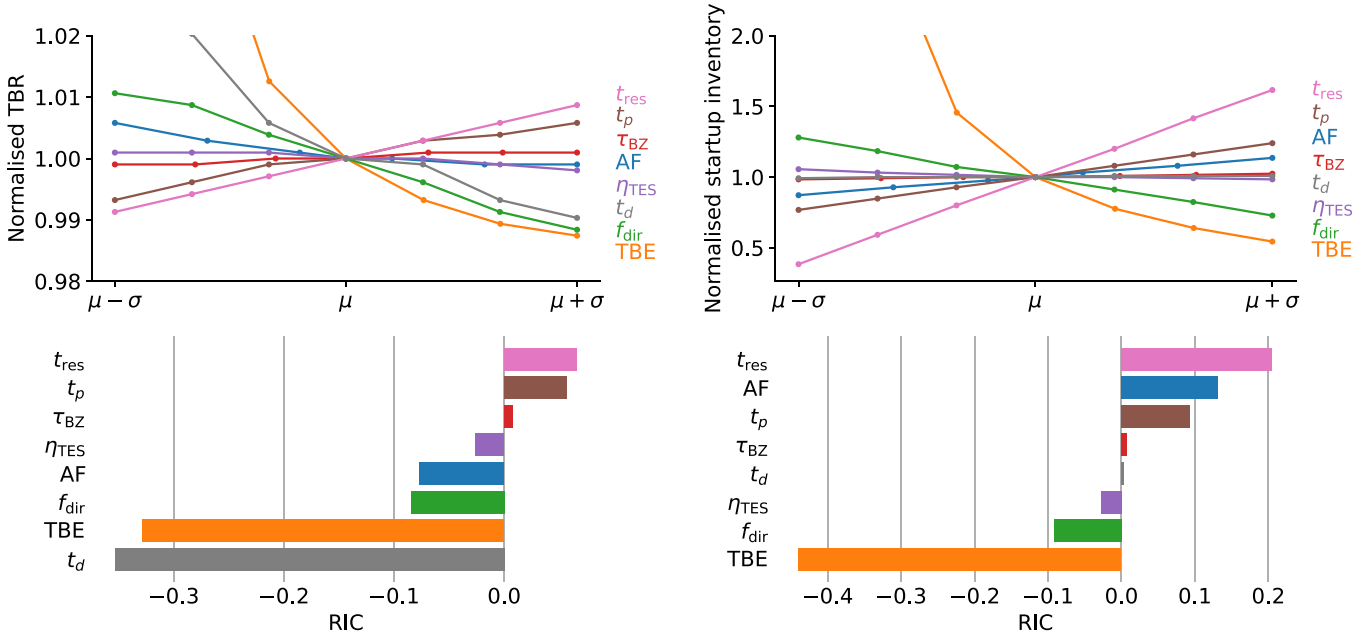

(a) TBR (b) Start-up inventory

Figure 5. (*a*) Normalized TBR and relative sensitivity index coefficient (RIC) show the sensitivity of TBR_r to the eight parameters listed in table 5. (*b*) Normalized I_{startup} and RIC show the sensitivity of I_{startup} to the same eight parameters. To normalize $\mathrm{TBR_r}$ and I_{startup}, all design parameters were set to the mean value reported in table 5. Each design parameter has been varied in $[\mu-\sigma, \mu+\sigma]$, where σ is the range reported in table 5. Both $\mathrm{TBR_r}$ and I_{startup} sharply increase as TBE decreases. TBE shows the second largest (by absolute value) RIC for TBR_r and the largest RIC for I_{startup}. With the exception of AF, the RIC for each design parameter has the same sign for $\mathrm{TBR_r}$ and I_{startup}, meaning that the minimization of $\mathrm{TBR_r}$ and I_{startup} can be achieved without tradeoffs. AF considerations are explained in detail in section 3.7.

where IC_i is the sensitivity index coefficient of the ith parameter and the summation runs over all parameters.

The most impactful parameters for $\mathrm{TBR_r}$ are TBE and the doubling time t_{d}. $\mathrm{TBR_r} \to \infty$ as $\mathrm{TBE} \to 0$ because the fuel utilization is so low that the amount of bred tritium is negligible relative to the I_{startup} that must be doubled. This limit also follows from the definition of the fuel injection rate $\dot{T}_{\mathrm{fuel}}$:

$$\dot{T}_{\mathrm{fuel}} = \frac{\dot{N}_{\mathrm{T,burn}}}{\mathrm{TBE}}. \tag{46}$$

As $\mathrm{TBE} \to 0$, $\dot{T}_{\mathrm{fuel}} \to \infty$ (at fixed $\dot{N}_{\mathrm{T,burn}}$), and so the required $I_{\mathrm{startup}} \to \infty$ as well (figure 5). It is therefore impossible to meet a given target t_{d} unless $\mathrm{TBR} \to \infty$. Similarly, $\mathrm{TBR_r} \to \infty$ as $t_{\mathrm{d}} \to 0$. In order to achieve both tritium self-sufficiency and shorter t_{d}, it is necessary to achieve high TBE. Other factors that impact $\mathrm{TBR_r}$—although not to the extent that t_{d} and TBE do—include:

- DIR fraction f_{DIR}: affects IFC dynamics. Higher DIR fractions reduce the time tritium spends in the IFC, decreasing I_{startup} and $\mathrm{TBR_r}$;
- Reserve time t_{res}: a larger t_{res} requires a larger I_{startup} and thus a higher $\mathrm{TBR_r}$ (given a fixed t_{d});
- Tritium processing time t_{p}: affects IFC dynamics in a similar way to f_{DIR};
- AF: a lower AF indicates less operating time and less tritium production, so $\mathrm{TBR_r}$ must increase to meet the t_{d} target if AF decreases.

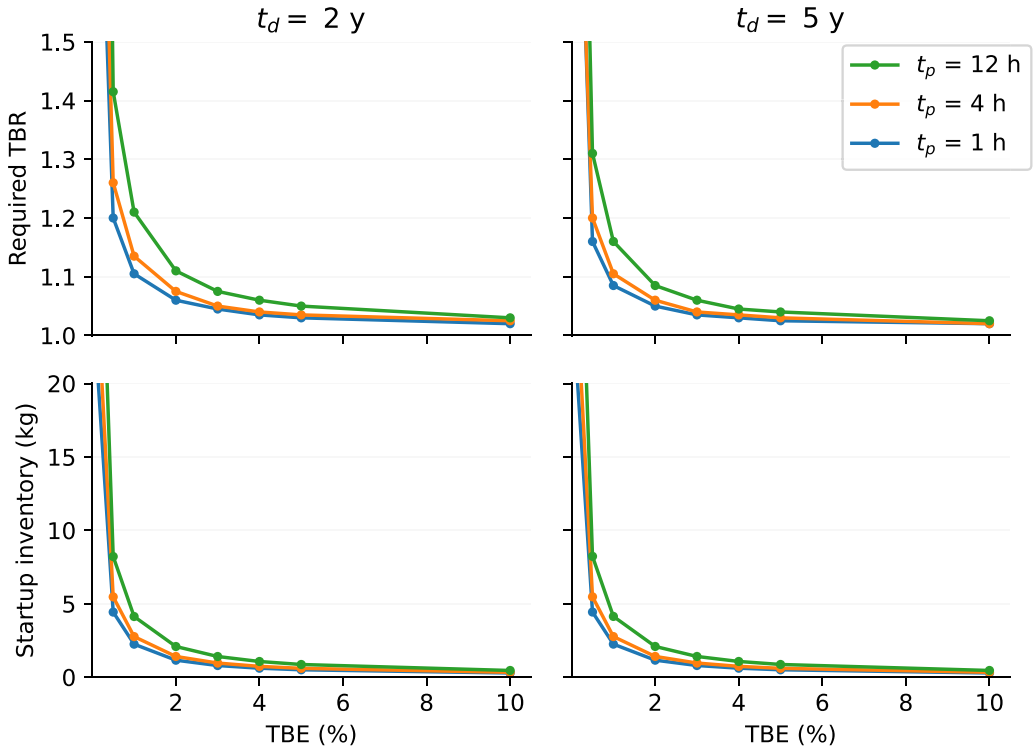

Figure 6. TBR_r and $I_{startup}$ as a function of TBE, for different processing times and doubling times. For $t_d = 2$ yr (left column), t_p has a small impact on TBR_r when TBE is high (>4%). For low TBE, tritium self-sufficiency becomes difficult to practically achieve unless t_p is quite low. For the longer t_d of 5 yr (right column), engineering and design constraints on the blanket are relaxed: tritium production rates can be lower and longer t_p is acceptable. The plots also show that for very low TBE < 0.5%, $I_{startup}$ and TBR_r sharply increase to impractical values.

τ_{BZ} and η_{TES} have a weak effect on TBR_r. While they affect the tritium inventory in the OFC, they do not significantly impact system dynamics and tritium production. This is explained in greater detail in sections 3.3–3.4.

3.3. TBE

TBR_r and $I_{startup}$ are shown in figure 6 as a function of TBE for different values of t_p. We consider it highly unlikely that we can attain TBR > 1.3; extremely challenging but possible to attain TBR = 1.2–1.3, challenging but reasonable to expect that we can attain TBR = 1.1–1.2, and very possible to achieve TBR < 1.1. The lowest value of TBE considered, 0.5%, might be a realistic value for the first generation of ARC-class tokamaks [77], but will require fast processing times and high TBR to achieve tritium self-sufficiency. For low values of TBE, t_p has a large impact on TBR_r and $I_{startup}$ because most of the injected tritium is exhausted from the vacuum boundary and processed in the IFC. Figure 6 highlights the importance of achieving high TBE and fast t_p in order to relax TBR requirements on the blanket design.

As TBE increases, less tritium is flowing through the IFC and the importance of t_p diminishes. In fact, the fueling injection rate decreases as TBE increases (equation (46)) while keeping fusion power fixed (i.e. fixed tritium burn rate). As a consequence, the tritium flow rate in the IFC decreases, thus decreasing $I_{startup}$ and TBR_r. Slow IFC dynamics ($t_p > 4$ h) are acceptable for TBE > 4%, and $TBR_r < 1.1$ and $I_{startup} < 2$ kg are still within reach. Figure 6 shows that targeting a longer t_d is an effective way to reduce TBR_r. However, $I_{startup}$ is weakly affected by the choice of t_d, and other strategies are needed to decrease it.

3.4. OFC residence time

The relevant timescales for tritium transport through the OFC range from a few minutes in the divertor, FW, and HX to days in the breeding zone and TES. OFC dynamics are therefore dominated by τ_{BZ} and τ_{TES}. The baseline case assumes τ_{BZ} = 1.25 h and τ_{TES} = 24 h. The components with a short tritium residence time do not significantly affect nominal system operations, even if the residence time is increased by a factor of 10 (i.e. from 20 min to 3 h). Figure 7 shows how different values of τ_{BZ} affect TBR_r and $I_{startup}$. Decreasing τ_{BZ} does not have a significant impact on TBR_r or $I_{startup}$ for $\tau_{BZ} < 24$ h. As τ_{BZ} goes above 1 d, there is a small corresponding increase in TBR_r and $I_{startup}$. Generally, as long as τ_{BZ} is on the order of 1 d, engineering efforts directed at decreasing τ_{BZ} are unlikely to meaningfully reduce TBR_r or $I_{startup}$.

Figure 8 shows the evolution of tritium inventories in the ISS, tritium storage, breeding zone, and TES systems for τ_{BZ} = 1 h and τ_{BZ} = 10 d. Longer values of τ_{BZ} are associated with a larger breeding zone inventory and a delayed inflection point. In figure 8, the increase in τ_{BZ} shifts the inflection point time from ∼hours after start-up to ∼days. Nevertheless, this shift is negligible compared to the doubling time, and increasing τ_{BZ} results in very small increases in TBR_r. The observed increase in TBR_r compensates for the

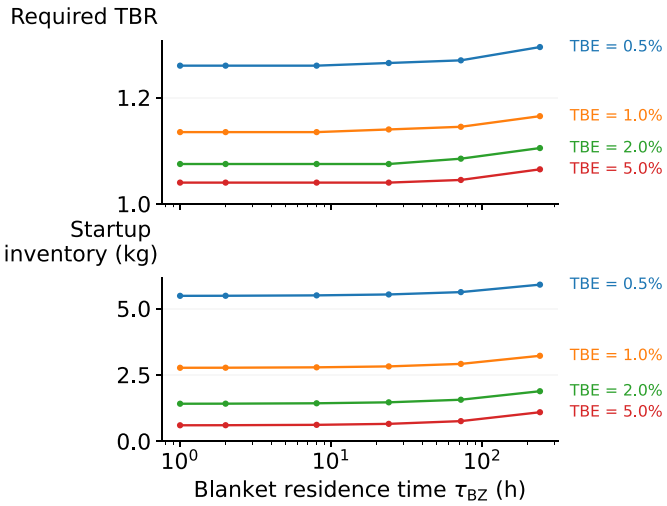

Figure 7. TBR_r and $I_{startup}$ for different residence times in the breeding zone. τ_{BZ} has effectively no impact on TBR_r and $I_{startup}$ for $\tau_{BZ} < 1$ day. At longer τ_{BZ}, TBR_r and $I_{startup}$ increase slightly.

larger tritium losses in the breeding zone that inevitably occur (e.g. due to permeation or radioactive decay) when tritium resides there for longer.

Figure 9 shows the steady-state breeding zone inventory for different residence times. This relationship is linear. A τ_{BZ} of 10 d results in a steady-state breeding zone inventory of ~600 g; for $\tau_{BZ} = 1$ h, this drops to ~3 g. Here we see the advantage of efficient T extraction from the blanket: while τ_{BZ} may not have a large impact on TBR_r or $I_{startup}$, it determines T inventory in the blanket. Large quantities of tritium in any part of the plant present maintenance challenges and may be unacceptable from a regulatory standpoint: we want to attain tritium self-sufficiency while still minimizing overall on-site inventory.

τ_{TES} and τ_{BZ} have the same effects on the OFC dynamics and tritium self-sufficiency. Varying τ_{TES} results in equivalent inventory evolution trends as those shown in figures 7 and 8, and the plotted results are omitted here.

3.5. *Tritium extraction efficiency*

The OFC is further characterized by the TES tritium extraction efficiency η_{TES}. It is difficult to assume a baseline value for η_{TES} for ARC because tritium extraction from FLiBe has been poorly investigated [52, 82], extrapolation from small scale experiments is not straightforward, and full-scale breeding systems have not been tested yet. Experimental data on tritium solubility and diffusivity in FLiBe is limited in scope and varies by multiple orders of magnitude [71]. In this work, η_{TES} is varied over a wide range to explore the consequences of multiple operating points for an ARC-class plant. Data from the upcoming LIBRA experiment will narrow the range of possible values of η_{TES} for an ARC-class FPP [31].

Counterintuitively, η_{TES} does not have a strong impact on tritium self-sufficiency. If η_{TES} is lowered, the concentration of tritium in the FLiBe of the ARC breeding zones increases, but the rate of tritium extraction is maintained at the prior level.

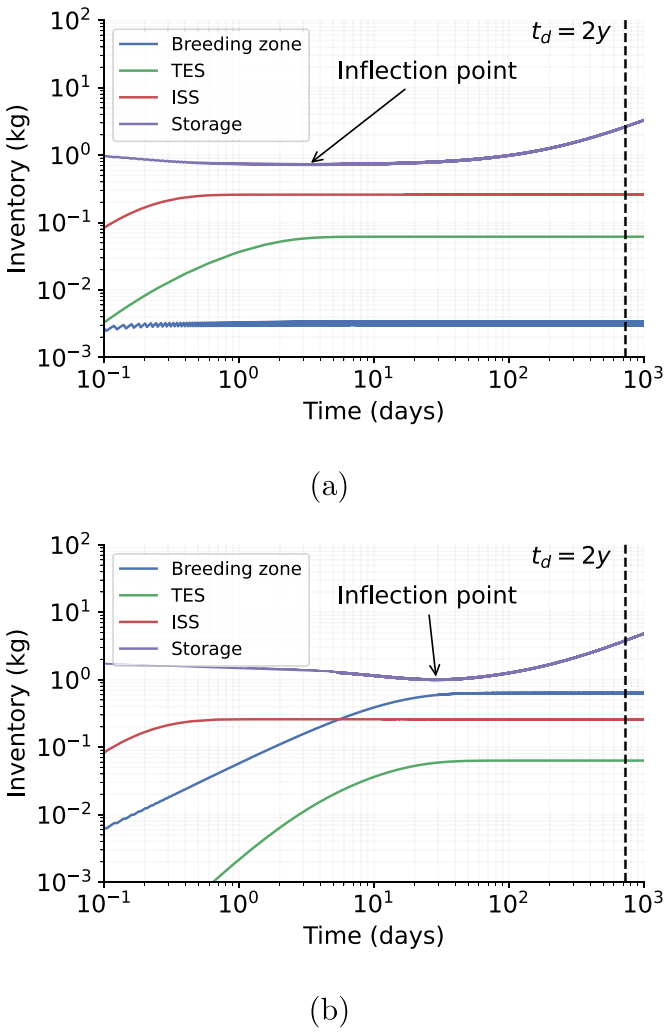

Figure 8. Evolution of relevant system inventories for (*a*) $\tau_{BZ} = 1.25$ h and (*b*) $\tau_{BZ} = 10$ d. The slower dynamics and the shift of the inflection time for $\tau_{BZ} = 10$ d is evident.

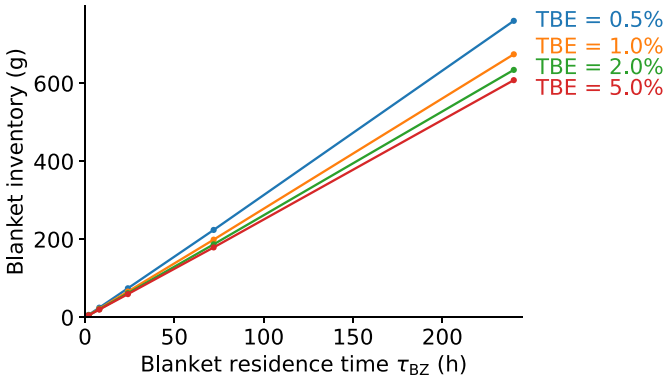

Figure 9. Steady-state tritium inventory in the breeding zone for different residence times. Longer τ_{BZ} is associated with larger T inventories in the blanket, which presents maintenance and regulatory challenges. Higher values of TBE are associated with smaller tritium inventories in the breeding zone, as the fuel is being used more efficiently and TBR_r is lower.

This affects the tritium inventories in the OFC (higher tritium concentrations in FLiBe lead to higher concentrations in the other OFC components), but not self-sufficiency. The OFC

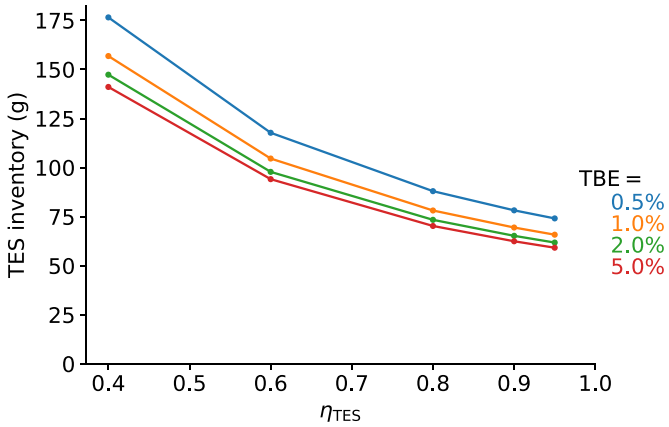

Figure 10. Steady-state tritium inventory in the TES for different values of η_{TES} and TBE. Higher efficiency in the TES and in the fueling system corresponds to lower TES tritium inventory.

components take more time to reach their steady-state tritium inventory values, but TBR_r remains almost the same. We have explained in section 3.2 how the TBR_r is strictly related to t_d. The slowing of OFC dynamics is negligible with respect to the doubling time (days vs years). Furthermore, the additional tritium lost due to buildup in the OFC components (10–100 g, as shown in figure 10) is 1–2 orders of magnitude smaller than the initial inventory that must be doubled (1–10 kg). The TES tritium inventory for different values of η_{TES} is shown in figure 10. Even in the worst-case scenario (TBE = 0.5%) the difference between a high efficiency TES ($\eta_{TES} = 95\%$) and a low efficiency TES ($\eta_{TES} = 40\%$) is a ~100 g increase in the TES inventory. η_{TES} has a marginal effect on TBR_r. For TBE = 1%, if we reduce η_{TES} from 95% to 40%, TBR_r increases from 1.15 to just 1.16—less than a 1% increase.

3.6. Direct internal recycling fraction

DIR only impacts the IFC dynamics. As was also the case for the DEMO FC in [1], the inclusion of a DIR line can have a dramatic impact on TBR_r and $I_{startup}$ in the ARC FC if operating at low TBE values. DIR technology is therefore an important tool for achieving tritium self-sufficiency, especially if fueling technologies are not significantly improved by the time the first FPPs are built. A DIR fraction of 0.9 (indicating that 90% of exhausted fuel is directly recycled back to tritium storage and fueling) reduces TBR_r by 10% for TBE = 0.5% . The TBR_r reduction is less dramatic when operating with high-efficiency fueling: at higher values of TBE, the tritium flow rate in the IFC is decreased, thus reducing the impact of DIR on TBR_r. For example, at TBE = 5%, implementing DIR with $f_{DIR} = 0.9$ reduces TBR_r by just 1%. This relationship between TBR_r and f_{DIR} is shown in figure 11(*a*). $I_{startup}$ follows a similar trend: increasing f_{DIR} decreases $I_{startup}$, but the trend is most pronounced at low TBE values. $I_{startup}$ is strongly affected by IFC dynamics because the majority of tritium in the plant will flow through the IFC (95% for TBE = 5%).The DIR line is therefore also a powerful tool for reducing $I_{startup}$ and easing regulatory burdens for ARC. However, including DIR leads to

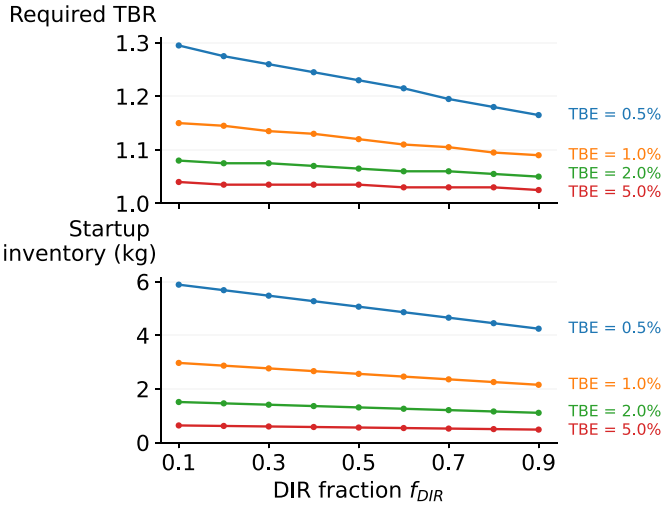

Figure 11. TBR_r and $I_{startup}$ as a function of the direct internal recycling fraction. DIR is more advantageous when operating at low tritium burn efficiency.

a more complex IFC design. If ARC is able to achieve high TBE, the increase in system complexity may not be worth the small reduction in $I_{startup}$ and TBR_r (especially for low f_{DIR}).

3.7. AF

FPPs must reliably output power to be economically feasible. It is explained in [1] that the mean time between failures in DEMO and the mean time to repair will be respectively short (on the order of days) and long (on the order of months). This is because the DEMO blanket, FW, and divertor are located inside the VV, which makes reliability, accessibility, maintainability, and inspectability (RAMI) quite complex for these components. Here, we see a key advantage of the ARC-class FPP. The VV is located inside the LIB, which uses a minimum of structural materials. This has important consequences for RAMI. The liquid blanket is not damaged by neutron radiation, cannot fail due to thermo-mechanical stresses, and provides a large thermal sink in case of severe accidents. Furthermore, demountable magnet coils and a drainable blanket allow easy access to the VV for maintenance and replacement[13]. In-vessel components can be removed and replaced without dismantling a great number of solid structural components, reducing MTTR. Ideally, these design choices will increase the AF of ARC-class FPPs relative to other designs, as AF is inversely proportional to MTTR (equation (24)).

The effect of plant AF on TBR_r is shown in figure 12. Improving AF has the most significant impact on reducing TBR_r when TBE is low. The two dashed lines identify the best-case AF operating points for two possible combinations of (t_{pulse}, t_{off}). For ($t_{pulse} = 1800$ s, $t_{off} = 60$ s) the best possible

[13] In ARC-class FPPs, the VV is not a lifetime component, but is replaced regularly (i.e. every few years). This eases the challenge of robust VV design, because the structure needs to retain its integrity for a shorter time.

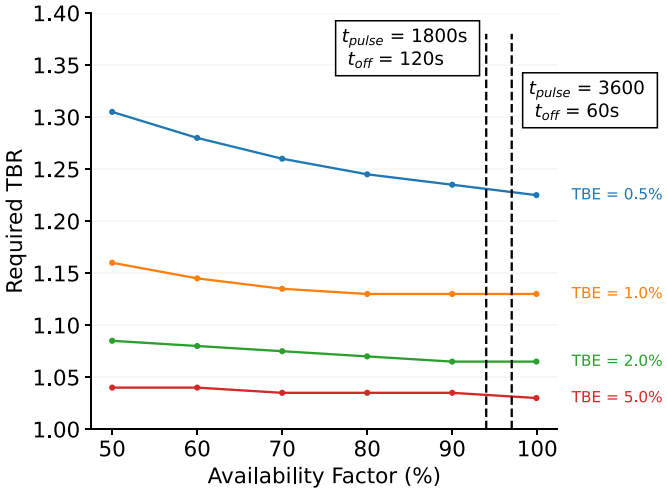

Figure 12. TBR_r as a function of availability factor (AF). The dashed lines identify the AF for two different combinations of t_{pulse} and t_{off}.

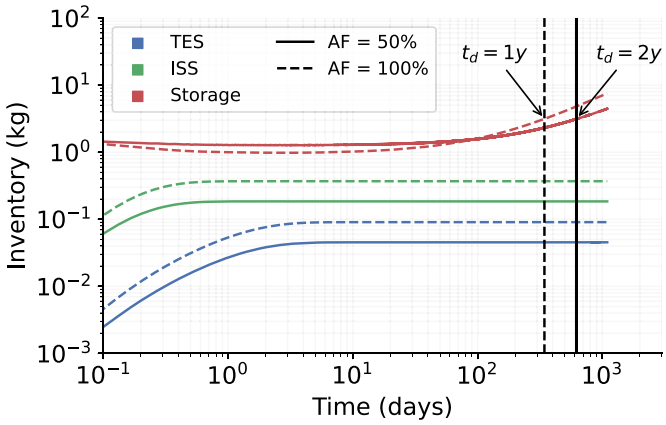

Figure 13. Evolution of the tritium inventories in the tritium extraction system, isotope separation system, and tritium storage system. These are the most relevant tritium inventories in the plant. At fixed TBR, an FPP with AF = 50% takes almost twice the time to double the initial inventory with respect to an FPP with AF = 100%.

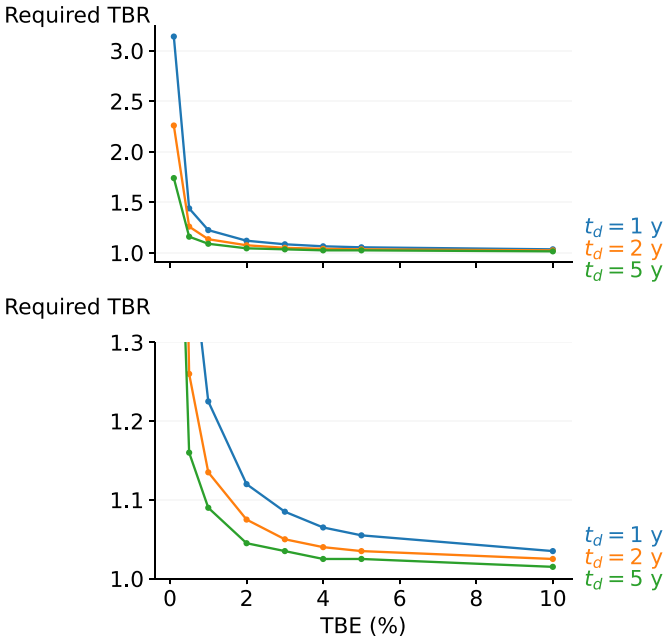

Figure 14. TBR_r for different doubling times t_d. A short t_d requires high TBR. For t_d = 1 yr, tritium self-sufficiency is highly unlikely if TBE < 1%. If a longer t_d is acceptable, tritium self-sufficiency is much easier to achieve. For t_d = 5 yr, tritium self-sufficiency is possible even if TBE = 0.5%. The bottom plot zooms in on TBR_r in the region of interest (TBR_r < 1.3).

AF (no system failures or need for maintenance) is 97%. For (3600 s, 120 s) the best possible AF is 94%.

At TBE = 0.5%, tritium self-sufficiency is almost impossible if AF < 90%: it is difficult to see, based on neutronics studies, how we could achieve a TBR > 1.25. In this scenario, a large DIR fraction would be required to bring down the TBR_r, and even then it is not obvious that tritium self-sufficiency would be possible. On the other hand, for TBE > 1%, tritium self-sufficiency could theoretically be achieved even with low availability factors, e.g. AF = 50% (although TBR_r > 1.15 is still not necessarily 'easy' to achieve). For TBE = 5%, TBR_r is almost insensitive to improvement in AF > 70%. Note that if AF drops below 50%, TBR_r increases significantly, as described in [1]. This is because at low AF, radioactive decay loss becomes significant (inventory will decrease at a rate of ~5.5% per year if the plant is not producing tritium). Furthermore, if t_d is fixed, more tritons must be produced for every neutron to compensate for the shorter operating window associated with low AF.

$I_{startup}$ is not affected by AF for any value of TBE. A lower AF shifts t_{infl} further in time (figure 13). However, even for AF = 50%, when t_{infl} is almost doubled, the timescales involved are of the order of days. The additional tritium required to compensate for the associated decay losses is negligible, and $I_{startup}$ does not increase when the AF decreases. So while improving AF will not reduce $I_{startup}$, high AF is necessary for faster t_d and, of course, reliable production of power.

3.8. Doubling time

The doubling time t_d is the most important parameter affecting TBR_r, and we assume the FPP is intentionally designed to be capable of achieving a target t_d. A shorter t_d requires a larger tritium production rate and a higher TBR. Conversely, tritium self-sufficiency requirements can be relaxed if a longer t_d is acceptable to the FPP designers. Figure 14 shows TBR_r for the ARC system for different doubling times. For TBE = 0.5%, FPP designers would likely need to settle for long doubling times (on the order of years) in order to get to a reasonably achievable TBR_r. If t_d = 5 yr is acceptable, then tritium self-sufficiency should not be a leading issue, especially if TBE > 1% (i.e. TBR_r < 1.1). It should be noted that short t_d (e.g. t_d < 2 yr) may not even be desirable in early plants if FPPs are slow to penetrate the electricity market. Rapidly doubling the tritium inventory every year without a corresponding demand could result in unnecessary regulatory

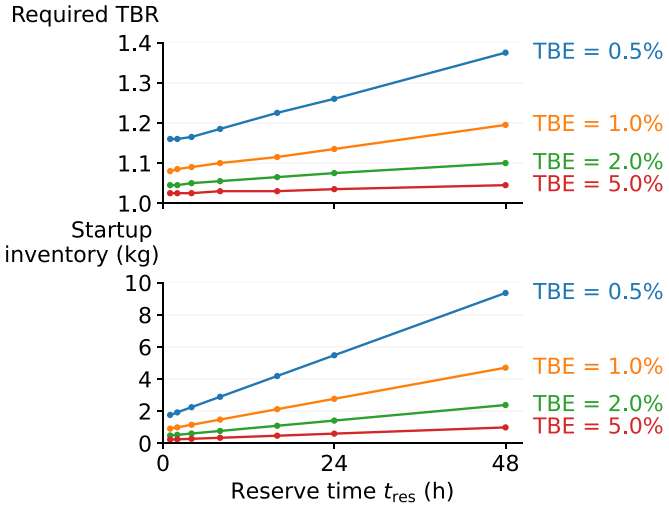

Figure 15. TBR_r and $I_{startup}$ for an ARC-class FPP as a function of tritium reserve time. $I_{startup}$ increases linearly with t_{res}. The TBR_r increases accordingly for fixed t_d as a higher inventory must now be doubled.

Table 6. TBR_r and $I_{startup}$ for an ARC-class FPP, assuming baseline design parameters, an ambitious operating scenario ($t_d = 1$ yr), and a moderately ambitious operating scenario ($t_d = 2$ yr). We consider how parameters change if we can implement significant improvements in FC technologies, in plasma operations (PO), or in both. The advanced-FC scenario considers AF = 90%, $f_{DIR} = 0.7$, $t_p = 1$ h, and TBE = baseline case (0.02, based on the current state-of-the-art). The advanced-PO scenario considers TBE = 0.1 and all other parameters unchanged from the baseline scenario. The 'both' scenario assumes that both FC and PO advances have been implemented.

	Baseline case	Ambitious ($t_d = 1$ yr)			Moderate ($t_d = 2$ yr)		
Parameters	No FC or PC advances	FC advances only	PO advances only	Both	FC advances only	PO advances only	Both
AF (%)	70	90	70	90	90	70	90
TBE (−)	0.02	0.02	0.1	0.1	0.02	0.1	0.1
f_{DIR} (−)	0.3	0.7	0.3	0.7	0.7	0.3	0.7
t_p (h)	4	1	4	1	1	4	1
t_d (y)	1 or 2	1	1	1	2	2	2
TBR_r (−)	1.113 ($t_d = 1$) 1.067 ($t_d = 2$)	1.064	1.029	1.022	1.039	1.017	1.012
$I_{startup}$ (kg)	1.14 ($t_d = 1$) 1.14 ($t_d = 2$)	1.12	0.33	0.30	1.12	0.33	0.30

challenges due to the need to safely store large amounts of tritium. For now, we assume that a target $t_d = 2$ yr is reasonable in terms of design requirements and possible benefits for a first generation of ARC-class FPPs.

3.9. Reserve time

The reserve time t_{res} has a fundamental impact on FPP operations in the event that some part of the FC fails. Longer reserve times make it possible to keep operating when failure requires a lengthy repair, but leads to higher $I_{startup}$ and thus higher TBR_r for a fixed t_d (figure 15). At TBE = 0.5%, $t_{res} > 24$ h is infeasible as this leads to unachievable TBR_r (>1.3). Improving TBE enables a longer t_{res}, but it is important to balance the advantages of a longer t_{res} against the disadvantages of a larger $I_{startup}$. At low values of TBE, small increases in t_{res} correspond to large increases in $I_{startup}$, as shown in figure 15.

3.10. Implications for ARC-class tokamak design and operations

Continued advances in both FC technology and plasma performance should make tritium self-sufficiency in ARC very feasible. However, the goal of this section is to provide design guidelines to ensure tritium self-sufficiency in the first generation of ARC-class FPPs even if minimal progress is made in FC or POs technologies in the coming years. Table 6 provides the TBR_r and $I_{startup}$ for an ARC-class FPP operating with an 'ambitious' FC (targeting $t_d = 1$ yr) and a 'moderate' FC (targeting $t_d = 2$ yr). For each, we consider three cases: (1) FC technology has improved significantly relative to the present day (but PO technologies have not), (2) PO technologies have improved significantly relative to the present day (but FC technologies have not), and (3) both the FC advances from (1) and the PO advances form (2) are implemented in a 'best case' scenario. In the model presented here, improvements in the FC

correspond to improvements in AF, f_{DIR}, and t_p. Improvements in PO correspond to improvements in TBE. Results in table 6 are based on a simplified view of a very complex engineering system, but they provides useful guidelines for organizing near-term R&D of ARC-class tokamaks. As was the case in [1] for DEMO, improving the TBE lowers the required AF, f_{DIR}, and t_p to achieve a given t_d target. For both the ambitious and moderate t_d targets, TBR_r is well within the expected achievable range (<1.15) if FC and PO technologies improve with respect to the baseline case. The neutronics analysis carried out by Bae *et al* [17] reported a $TBR_a = 1.053$ for an Inconel-718 VV in ARC. A similar result is reported in [11], which used a simplified neutronics model of an ARC-class plant and calculated a $TBR_a = 1.07$. We note that while TBR_r can be lowered by improving PO and FC technology, we can also increase TBR_a by optimizing plant design and materials choices (for example, if V-Cr-Ti alloys can be used for the VV, TBR_a may be as high as 1.2 [11]).

A second consideration involves the DIR, which should lower TBR_r and $I_{startup}$ for a given FPP design at the cost of increased complexity. We note that if the TBE is sufficiently high, advantages gained from DIR are small and may not be worth the associated costs. Furthermore, we note that successful implementation of DIR in ARC depends on the development of MFPs that process the exhaust flow. If DIR is deemed necessary in order to achieve tritium self-sufficiency, then this is an obvious argument in favor of prioritizing R&D of these pumps.

Lastly, the start-up inventories reported in table 6 are reasonably achievable for the first ARC-class FPP. The initial tritium inventory required to begin operations can be provided by present reserves [20].

4. STEP tritium self-sufficiency

This section repeats the FC analysis from section 3 for STEP, a FPP being developed by the UKAEA. The STEP FC shows similar design parameter as ARC, and so the results are presented more briefly here. The STEP FC analysis is considered for both the EBB and the liquid lithium blanket designs that are considered in the literature. These two designs do not necessarily reflect the official design currently under development at UKAEA. Nevertheless, it is instructive to consider tokamak designs different from ARC-class tokamaks. We refer to these FPP concepts as STEP-EBB and STEP-Li.

4.1. STEP-EBB

In a recent preliminary study on plasma and FPP parameters for an ST FPP carried out by Schoofs and Todd [4], three possible design variants for an ST FPP are identified: compact, balanced, and conservative. The compact design ($R_0 = 3.26$ m) exploits a high toroidal magnetic field ($B_{T,max} = 23$ T) at the expense of a lower predicted toroidal magnet lifetime (1.3 FPY). The conservative design ($R_0 = 5.01$ m) limits the magnetic field to the values expected in ITER and EU-DEMO ($B_{T,max} = 12$ T), which translates to lower neutron wall loading and improved magnet lifetime (∼3 FPY). The balanced design is a compromise between the compact and the conservative designs. These three design variants, described in table 7, are considered in this analysis of STEP's tritium self-sufficiency capabilities.

Table 7. Plasma and FPP parameters for three STEP-EBB variants: 1, compact; 2, balanced; 3, conservative [4].

Parameter	Variant			Units
	1 (Comp.)	2 (Bal.)	3 (Cons.)	
$B_{T,max}$	23	16	12	T
R_0	3.26	4.05	5.01	m
B_0	4.23	3.75	3.30	T
I_p	22	24	26	MA
$n_{e,0}$	2.11	1.51	1.07	10^{20} m^{-3}
T_0	33	35	37	keV
P_{fusion}	3.21	3.38	3.37	GW_{th}

STEP-EBB breeds tritium in an EBB [3]. The FLiBe molten salt breeder is encapsulated in pebbles in a gas-cooled packed bed. The pebble shell is made from porous ceramic material to enhance tritium diffusion through the shell and to improve tritium extraction. A metallic jail surrounds the ceramic shell and prevents contact between the pebbles. The pebbles include a gas pocket for the tritium and helium produced in the FLiBe during neutron irradiation. Nitrogen flows between pebbles in the packed bed, providing cooling and tritium extraction.

4.1.1. STEP-EBB FC.

A tentative block diagram of STEP is proposed in figure 16. Since the methodology exploited for the analysis is high-level, most of the blocks are identical to those of an ARC-class FPP (see section 2.2). In principle, there are no differences in the IFC layout of STEP- and ARC-class FPP. The higher exhaust stream in STEP ($P_{fus,STEP} \sim 6P_{fus,ARC}$) may result in a different choice of IFC technologies, but these considerations are premature due to the conceptual nature of the STEP and ARC designs.

However, the OFC layout of the STEP-class FPP is different from the ARC-class FPP OFC. The STEP-EBB breeder (FLiBe) and the breeding blanket (pebble bed) are modeled as two different components in figure 16 because the tritium extraction process takes place in two steps. Tritium is produced in the FLiBe, which is encapsulated in the pebbles. This tritium is initially extracted by the purge gas (N_2). The TES then separates tritium from the nitrogen purge gas and the helium produced by the $^6Li(n,t)^4He$ reactions. Furthermore, the HX present in the ARC-class OFC is replaced by a turbine in the STEP-class OFC to enable a direct power generation cycle [3].

We assume that the tritium residence time in the EBB is driven by diffusion of T in FLiBe. The porous pebble shell thickness is significantly smaller than the diameter of breeding material in the pebble (0.15 cm vs 0.925 cm) and the

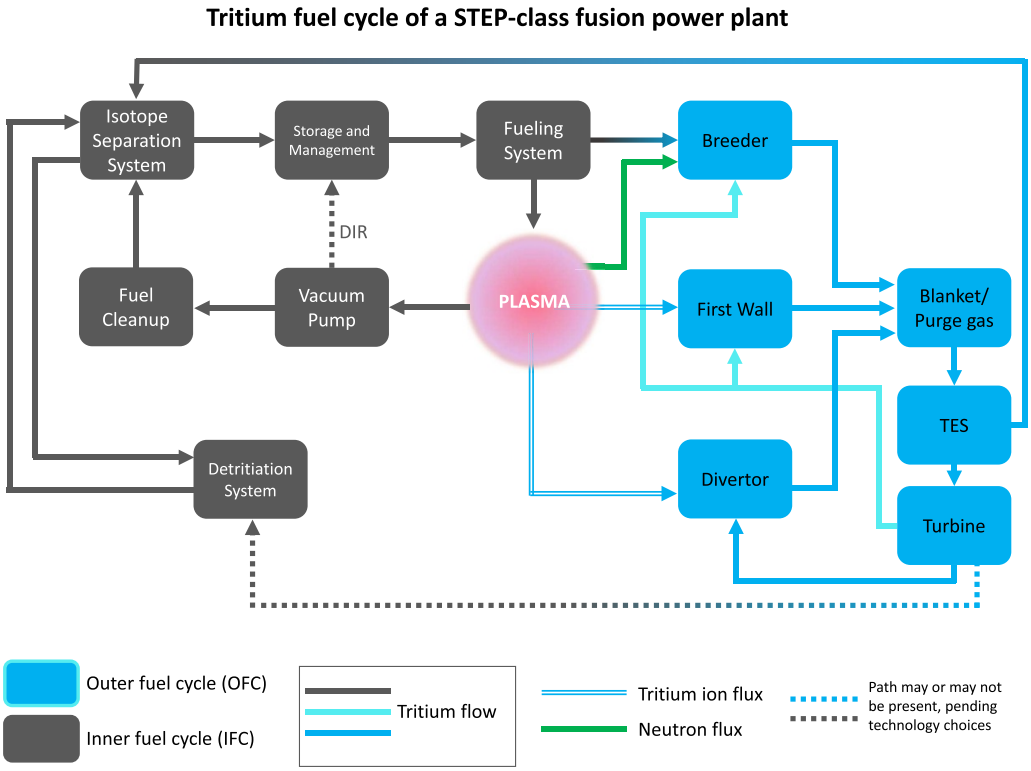

Figure 16. Fuel cycle block diagram for the STEP FPP. The DIR dotted path is present if the DIR is implemented in the IFC ($f_{\mathrm{DIR}} > 0$ in the model). The dotted path from the turbine to the detritiation system may be necessary to limit tritium losses from the turbine (for example, the turbine may be kept in a confined environment with a venting system connected to the detritiation system). The breeder (FLiBe in the pebbles) and the purge gas (N_2) flowing in the blanket modules are modeled by two separate blocks to more accurately model tritium extraction from the pebbles. The turbine replaces the heat exchanger to enable a direct power generation cycle [3].

metallic jail has no significant effects on tritium transport [3]. The characteristic time of T diffusion in FLiBe τ_{diff} can be estimated as:

$$\tau_{\mathrm{diff}} \sim \frac{L_{\mathrm{diff}}^2}{D_{\mathrm{T,FLiBe}}} \sim \frac{r_{\mathrm{pebble}}^2}{D_{\mathrm{T,FLiBe}}} \tag{47}$$

where L_{diff} is the characteristic length of T diffusion in FLiBe, $D_{\mathrm{T,FLiBe}}$ is the tritium diffusion coefficient in FLiBe [83] at an average FLiBe temperature of 915 K [3], and r_{pebble} is the pebble radius [3]. Equation (47) gives an estimated breeder residence time of approximately 6 h. Once the bred tritium reaches the purge gas flow, the EBB tritium residence time is dependent on the purge gas residence time (i.e. on the fluid dynamics of the N_2 flow). Nitrogen velocity in the blanket should be high enough to provide adequate cooling (an inlet velocity of $10\,\mathrm{m\,s^{-1}}$ is assumed in [3]), so the residence time in the blanket (τ_{bl}) should be of the order of minutes. We conservatively assumed $\tau_{\mathrm{bl}} = 1$ h. The TES must separate T from the N_2 carrier and from the He that inevitably permeates through the porous shell. No TES technology has been selected for STEP, but a similar technology to the cryogenic molecular sieve bed proposed for the EU-DEMO HCPB is assumed [84]. Therefore, the tritium residence time in the TES is assumed to be 24 h as in [84]. The last block of the OFC is the turbine. A single-loop Brayton cycle has been proposed for the encapsulated breeder design of STEP [3]. The residence time for the turbine block is assumed to be 1000 s.

4.1.2. Tritium self-sufficiency in STEP-EBB. The FC analysis for STEP-EBB followed the same approach as the ARC analysis. $\mathrm{TBR_r}$ and I_{startup} are computed for different FPP parameters and for the three design variants outlined in table 7. From the modeling point of view, TBE is the only significant difference between the three STEP-EBB variants. A TBE of 2% (advanced-FC scenario) and 10% (advanced-PO scenario) is considered for variant 1 (compact STEP-EBB) to keep the analysis consistent with the values assumed for ARC-class FPPs. To calculate TBE for variants 2 and 3, the value of TBE for variant 1 was used as reference value and we exploited the analytical expression for the TBE from [85] to compute the TBE ratio between two variants:

$$\mathrm{TBE}_i = \mathrm{TBE}_1 \frac{(\tau_p^* n_0 T_0^2 I_{\mathrm{fus}})_1}{(\tau_p^* n_0 T_0^2 I_{\mathrm{fus}})_i} \tag{48}$$

where $\tau_p^* = \frac{\tau_p}{1-R}$, τ_p is the particle confinement time, R is the particle recycling coefficient, I_{fus} is the fusion reactivity integral defined in equation (5) of [85], n_0 is the electron density (in 10^{20} $\mathrm{m^{-3}}$ units), and T_0 is the electron temperature (in keV). The same values for R, density, and temperature profile (obtained from [4]) were used for all three variants.

Table 8. TBR_r and $I_{startup}$ for STEP-EBB considering improvements in fuel cycle technologies (FC), plasma operations (PO) and both. The FC scenario considers AF = 90%, $f_{DIR} = 0.7$, $t_p = 1$ h and a TBE equal to the baseline case. The PO scenario considers TBE = 0.1 and all the other parameters equal to the baseline scenario. Ambitious ($t_d = 1$ yr) and moderate ($t_d = 2$ yr) design goals are considered.

	Ambitious ($t_d = 1$ yr)			Moderate ($t_d = 2$ yr)		
Parameter	FC advances only	PO advances only	Both	FC advances only	PO advances only	Both
AF (%)	90	70	90	90	70	90
TBE (−)	0.02	0.1	0.1	0.02	0.1	0.1
f_{DIR} (−)	0.7	0.3	0.7	0.7	0.3	0.7
t_p (h)	1	4	1	1	4	1
t_d (y)	1	1	1	2	2	2
TBR_r (−)	1.065	1.03	1.022	1.04	1.018	1.012
$I_{startup}$ (kg)	7.20	2.36	2.20	7.50	2.36	2.20

According to equation (48), $\frac{TBE_{variant1}}{TBE_{variant2}} = 0.001$, and $\frac{TBE_{variant1}}{TBE_{variant3}} = 0.007$.

The impact of these small differences on the results is negligible, so FC analysis results are reported for the compact STEP-EBB variant 1 only.

We again consider a total of six scenarios for STEP-EBB (Variant 1). For both an ambitious operating regime ($t_d = 1$ yr) and a moderate operating regime ($t_d = 2$ yr), we consider three scenarios: advanced FC, advanced POs, and both, following the definitions used for the ARC analysis in section 3. Assuming that the achievable TBR for STEP-EBB is ≈1.1, based on the breeding blanket optimization carried out in [3], we find that tritium self-sufficiency is achieved in five of the six scenarios. These are outlined in table 8. There exists a good margin between TBR_r and TBR_a (∼3%) even in the 'worst' case of the five scenarios that achieve tritium self-sufficiency (FC advances only, $t_d = 2$ yr). These results suggest that tritium self-sufficiency can be achieved even for small TBE in STEP-EBB if $t_d = 2$ yr is an acceptable target.

Of the five self-sufficient scenarios, the STEP-EBB start-up inventory ranges from 2.2 to 7.5 kg (this is large compared to ARC, but it is important to remember that STEP-EBB is a ∼3 GW_{th} plant). Improving TBE results in dramatic improvements to the required $I_{startup}$. Even small increases of TBE could lower the start-up inventory below 10 kg, which may be an acceptable value for a FOAK spherical tokamak FPP.

A sensitivity analysis has been carried out for STEP-EBB using the same parameters and value ranges given in table 5, with one exception. This is the breeder residence time τ_{BZ}, which has a mean value of 6 h and $\sigma = \pm 5$ h (compared to 13±11 h for the ARC-class tokamak). Results from this sensitivity analysis are shown in section 5, which compares results for both the STEP and ARC-class plants.

4.2. STEP-Li

A possible alternative to the EBB is a liquid lithium breeding blanket. Liquid lithium is not affected by irradiation damage, and it is an effective coolant with low density and high thermal conductivity [86]. However, in contrast to FLiBe, liquid Li will interact more strongly with the magnetic field in the tokamak, resulting in larger pressure losses due to magneto-hydrodynamics (MHD) effects [87]. The residence time of tritium in the STEP-Li breeding zone is highly uncertain, as relevant experimental data is very limited.

Tritium extraction from a liquid lithium carrier is better understood. Tritium extraction from PbLi has been investigated in depth for EU-DEMO [48–50], providing possible values for η_{TES}. Therefore, a detailed two-parameter sensitivity analysis (τ_{BZ} and η_{TES}) is performed in this paper for STEP-Li to account for uncertainties in the estimation of TBR_r and $I_{startup}$.

4.2.1. STEP-Li FC.

The IFC of STEP-Li does not differ, in principle, from those of STEP-EBB or the ARC-class tokamak. Since the liquid lithium works as both coolant and tritium carrier, the OFC block diagram is equivalent to the ARC-class OFC shown in figure 1. However, τ_{BZ} and the chosen tritium extraction technology (and thus η_{TES}) are expected to be quite different. MHD effects in the STEP-Li blanket might increase τ_{BZ} relative to the FLiBe LIB. Our analysis accounts for this by exploring a much wider range of possible τ_{BZ}, from 1 h to 240 h. As for the TES, two possible technologies are considered: permeator against vacuum (PAV) and liquid–liquid extraction (LLE). The PAV has been extensively investigated for the DEMO designs using PbLi breeder [48–50]. The estimated η_{TES} spans from 3% to 80% in those works, resulting in a second large source of uncertainty. The tritium extraction efficiency for the LLE as assumed by [51] is 20%. We considered η_{TES} from 3% up to 100% to be consistent with the analyses carried out for ARC and STEP-EBB. However, we performed a more in-depth sensitivity analysis on τ_{BZ} and η_{TES} for STEP-Li to assess the uncertainties on TBR_r and $I_{startup}$.

4.2.2. Tritium self-sufficiency in STEP-Li.

The fusion power and tritium burn rate for STEP-Li was assumed to be the same as STEP-EBB. The two-parameter sensitivity analysis has been carried out by randomly sampling τ_{BZ} from 1 to 240 h and η_{TES} from 0.03 to 1. A FC simulation was run for each pair of randomly sampled parameters, for a total of 100 simulations. Since the 100 simulations cover only a small part of the possible design space, TBR_r was fitted by a Gaussian process regression (GPR) model [88]. A GPR model is particularly advantageous because it allows us to fit and compute the mean and standard deviation of the target variable (TBR_r) via linear

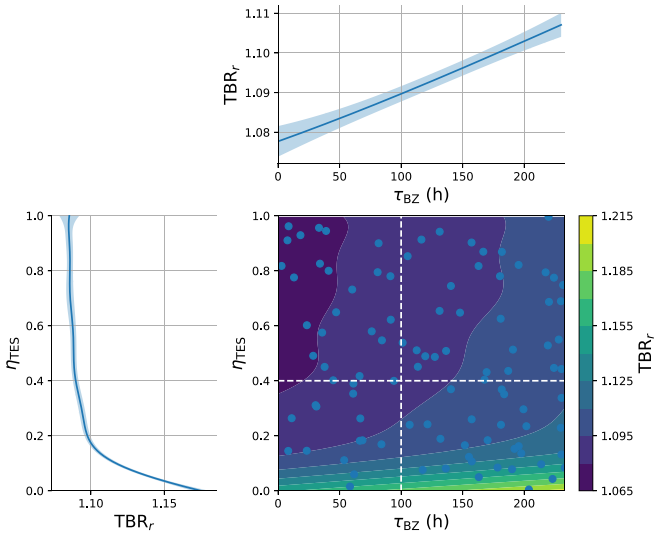

Figure 17. Contour map for TBR$_r$ in STEP-Li as a function of the blanket residence time τ_{BZ} and the TES efficiency η_{TES}. Blue markers identify simulated points in the design space. η_{TES} significantly impacts TBR$_r$ only at very low values ($\eta_{TES} < 0.1$). The impact of τ_{BZ} is stronger. Most of the variation for TBR$_r$ is found at very low values of η_{TES} and very high values of τ_{BZ} (bottom right corner).

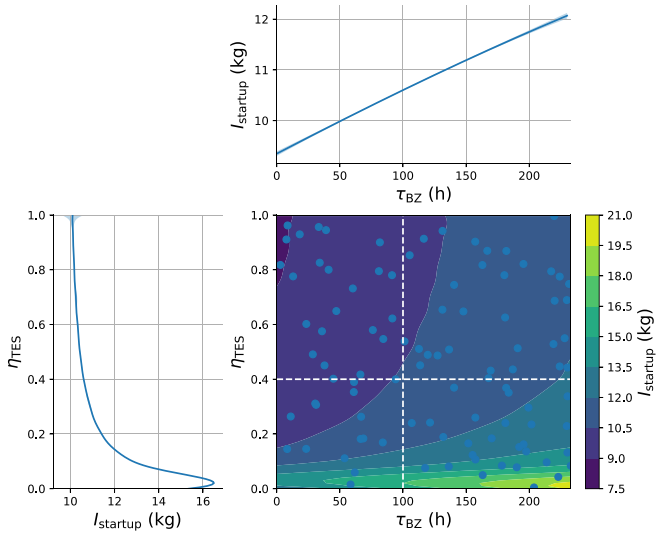

Figure 18. Contour map for $I_{startup}$ in STEP-Li as a function of the blanket residence timeτ_{BZ} and the TES efficiency η_{TES}. Blue markers identify simulated points in the design space. $I_{startup}$ is significantly impacted by η_{TES} only for $\eta_{TES} < 0.1$. The impact of τ_{BZ} on $I_{startup}$ is slightly stronger. $I_{startup}$ can increase up to 21 kg (i.e. ~100% increase from the minimum achievable value) for very low η_{TES} and extremely long τ_{BZ} (bottom-right corner).

regression, i.e. $\vec{y} = \vec{x}^T\vec{\beta} + \vec{\epsilon}$, where ϵ is normally distributed. According to these results, there exists 95% probability that the TBR$_r$ will be within $\pm 2\sigma \sim \pm 0.015$ of its calculated mean value. This approach allowed to properly account for the huge uncertainty of τ_{BZ} and η_{TES} in STEP-Li, whose liquid lithium blanket has not been modeled yet with the same level of detail of ARC blanket [14] or STEP-EBB blanket [3]. The other FC parameters were equivalent to those used in the baseline case for the ARC-class tokamak described in table 3.

Results from the GPR fit are reported in figure 17. The contour plot shows the required TBR as a function of τ_{BZ} and η_{TES} in STEP-Li. The required TBR ranges from 1.07 to 1.21. The lowest value is achieved in a wide area defined by $\tau_{BZ} < 100$ h and $\eta_{TES} > 0.3$. Very long τ_{BZ} or very low η_{TES} increase TBR$_r$ up to 1.21, close to the upper limit of what is expected for TBR$_a$. In general, though, blanket residence time and TES efficiency have relatively limited effect on TBR$_r$ outside of edge cases. It is important to emphasize that tritium solubility in liquid Li is significantly higher compared to its solubility in PbLi or FLiBe [83, 89, 90]. Consequently, while the extraction efficiency of different technologies remains highly uncertain, it is reasonable to anticipate lower extraction efficiencies (and, consequently, larger tritium inventories in the OFC) when extracting tritium from liquid Li compared to a tritium carrier like PbLi or FLiBe.

The start-up inventory contour map for STEP-Li is shown in figure 18. $I_{startup}$ ranges from 9 kg to 21 kg. An almost linear dependence on τ_{BZ} is observed due to the definition of residence time (blanket tritium inventory increases linearly with the tritium residence time in the blanket). A weak dependence on η_{TES} is observed except for very low values of η_{TES}, which result in large TES inventory. Figure 18 shows the mean and variance of the predicted $I_{startup}$ for STEP-Li, as computed by the GRP model. Based on this analysis, there is 95% probability that $I_{startup}$ will be within $\pm 2\sigma \sim \pm 30$ g of the calculated mean.

TBR$_r$ and $I_{startup}$ are computed for the three technology scenarios (FC advances, PO advances, and both) under ambitious and moderate t_d targets. These results are described in table 9 and are found to be quite similar to the STEP-EBB design. This is to be expected because the main modeling difference between STEP-EBB and STEP-Li in this analysis is blanket residence time (6 h for STEP-EBB vs 24 h for STEP-Li), which leads to an increase in $I_{startup}$ and, consequently, a small increase in TBR$_r$.

5. Discussion

The results suggest that, based on the current conceptual design of ARC-class and STEP-class tokamaks, tritium self-sufficiency will be possible. Section 5.1 compares the ARC FC results to those calculated for STEP-EBB and STEP-Li (in this work) and EU-DEMO (in [1]). Section 5.2 highlights the link between TBE and power production and shows why the TBE cannot be increased indefinitely. Section 5.3 briefly discusses the potential impact of tritium trapping, which has not been considered in this model. Section 5.4 highlights the next steps to increase the accuracy of FC modeling. Section 5.5 analyses the relationship between the tritium doubling time and FPP construction time.

5.1. Comparison of D-T FPP designs

The FC analysis for DEMO presented in [1] highlighted serious vulnerabilities in the design of the 3 GW$_{th}$ FPP

Table 9. TBR_r and $I_{startup}$ for STEP-Li considering improvements in fuel cycle technologies (FC), plasma operations (PO), and both. The FC scenario considers AF = 90%, $f_{DIR} = 0.7$, $t_p = 1$ h and a tritium burn efficiency equal to the baseline case. The PO scenario considers TBE = 0.1 and all the other parameters equal to the baseline scenario. Ambitious ($t_d = 1$ yr) and moderate ($t_d = 2$ yr) design goals are considered.

	Ambitious ($t_d = 1$ yr)			Moderate ($t_d = 2$ yr)		
Parameter	FC advances only	PO advances only	Both	FC advances only	PO advances only	Both
AF(%)	90	70	90	90	70	90
TBE(−)	0.02	0.1	0.1	0.02	0.1	0.1
$f_{DIR}(-)$	0.7	0.3	0.7	0.7	0.3	0.7
t_p (h)	1	4	1	1	4	1
t_d (y)	1	1	1	2	2	2
TBR_r	1.069	1.034	1.025	1.041	1.020	1.015
$I_{startup}$ (kg)	7.50	2.36	2.20	7.20	2.36	2.20

with regards to tritium self-sufficiency. For low TBEs (TBE = 0.36%) and fueling efficiencies ($\eta_{TES} = 25\%$) that currently characterize the technologies used in the design, TBR_r is far larger than the achievable TBR deemed possible by the inherent neutronics of the plant. If such a low TBE characterizes ARC- or STEP-class FPP, tritium self-sufficiency will be similarly unlikely.

In section 3.2 we showed how TBR_r is mostly determined by the t_d target, which is independent of the fusion power. Figure 19 shows the RIC for TBR_r and $I_{startup}$ for the three FPP designs. Practically no differences exist between ARC and STEP designs. Since the layouts of their IFCs are the same, and their OFC differs only for a few parameters, this is to be expected. The RIC for η_{TES} of STEP-EBB is almost null, probably due to the short timescale of its OFC (τ_{BZ}) as compared to ARC or STEP-Li. Figure 19 suggests that the results presented in this analysis are applicable to other tokamak designs with different OFC components, provided that $\tau_{OFC} \sim$ days and $\eta_{TES} > 10\%$ (otherwise tritium self-sufficiency changes drastically, as shown in figures 17 and 18).

Compact size, modular structure and the LIB concept bring many advantages to the ARC-class design. A very low availability factor is expected for DEMO and near-term FPP [1]. Therefore, a high TBE will be required to compensate for the low availability in order to achieve tritium self sufficiency. This will require major technology advances in a short time frame with regards to POs and fueling technologies. ARC-class tokamaks may be able to achieve much better availability factors from their first generation as a simple result of their characteristic design. Demountable magnets and a replaceable VV aim to minimize mean-time-to-repair and thus improve AF. The LIB can be considered a FPP lifetime component, which is undamaged by radiation damage or thermomechanical stresses. The maintenance required by the LIB is primarily chemistry control: FLiBe purity must be continuously monitored to prevent the formation aggressive radiochemical byproducts of the tritium breeding reaction (e.g, tritium fluoride) and remove impurities, as this is expected to cause severe corrosion issues in FLiBe-facing components. Of course, the successful operation of the ARC-class tokamak depends on the rapid development of demountable magnet joints and LIB technology. If this happens, it becomes realistic to target an availability factor larger than 50% in ARC, which will relax requirements on TBE . Similar considerations apply to STEP-Li, which features a liquid blanket. For STEP-EBB, the lifetime of the pebbles must be carefully assessed.

The lower fusion power of ARC does not directly lower TBR_r, but $I_{startup}$ is significantly lowered (table 10). We showed that $I_{startup}$ in ARC depends on the IFC dynamics and the desired reserve inventory (sections 3.6 and 3.9). Even if we assume that the FC dynamics of a STEP-class tokamak will be similar to those of ARC, the advantages of the ARC concept are clear. A 525 MW_{th} FPP burns much less tritium than a 3000 MW_{th} one. Hence, less tritium is required to sustain the initial operations of the FPP, and a lower reserve inventory is needed to account for possible FC failures. This translates to start-up inventories much lower than those required for STEP or DEMO (i.e. ∼1 kg vs ∼10–100 kg [1]). Table 11 lists the design parameters, TBR_r, and $I_{startup}$ for a 'worst-case' scenario for ARC, so-called because it assumes a low AF (below what would be targeted for commercial operation), no technological advances in burn efficiency, and no implementation of DIR. In this case, $TBR_r = 1.35$, above TBR_a for ARC, so improvements in the FC or in POs would be required to achieve at least the baseline design parameters in table 3 and to achieve tritium self-sufficiency. As far as the start-up inventory is concerned, $I_{startup} < 10$ kg even at TBE = 0.5%, $f_{DIR} = 0$, and AF = 50%. Considering that ARC is expected to start operations before ITER D-T operations, the initial tritium inventory for ARC can be covered by the available tritium supply [20]. Different conclusions apply to STEP-Li, which requires quite a large start-up inventory (figure 18(*b*) even for the baseline case. Improvements in FC dynamics and/or POs are therefore mandatory to lower STEP-Li start-up inventory to acceptable levels.

Large $I_{startup}$ does not need to be an unavoidable, intrinsic property of commercial FPPs. It can be minimized by relaxing constraints on the required tritium reserve inventory I_{res}, as shown in figure 20. This is evident for the advanced 'FC' scenario. I_{res} accounts for ≈85% of $I_{startup}$ in the STEP-class tokamak. The ARC start-up (and reserve) inventory is about 6× lower than STEP's because $P_{fus,STEP} \sim 6P_{fus,ARC}$. Without a reserve inventory, $I_{startup} < 200$ g. Decreasing or eliminating I_{res} is a key strategy for minimizing $I_{startup}$, and may be required

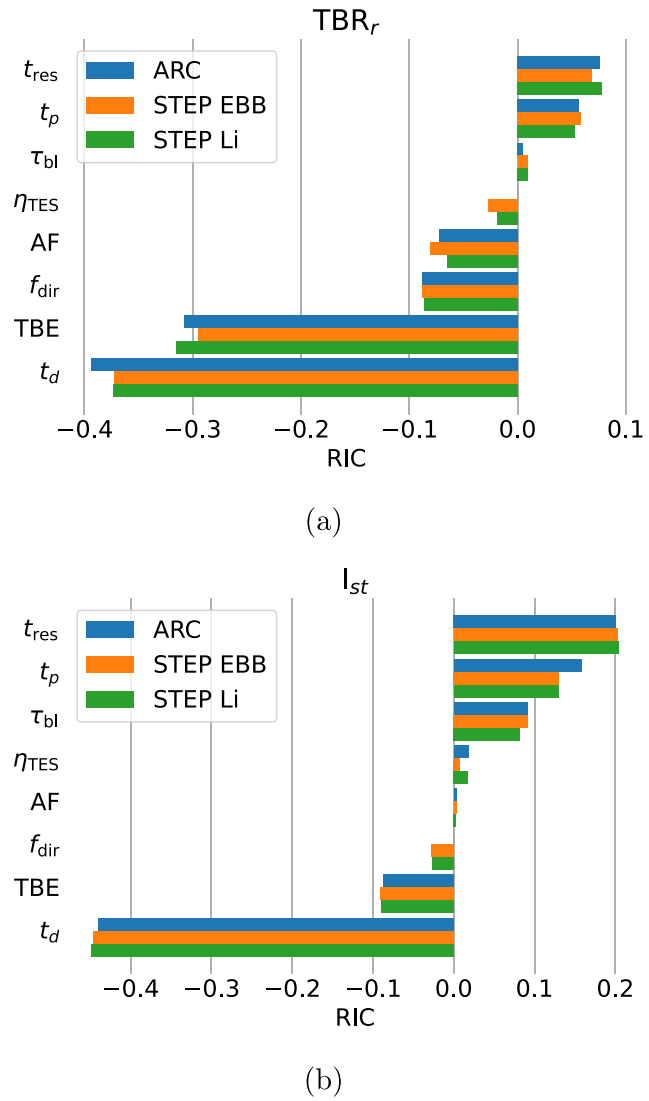

Figure 19. Relative sensitivity index coefficient (RIC) of TBR_r (*a*) and $I_{startup}$(b) of ARC, STEP-EBB and STEP-Li. No significant differences are found between ARC, STEP-EBB and STEP-Li as they have similar fuel cycle designs. $I_{startup}$ in STEP-EBB has a negligible dependence on η_{TES} due to the very short timescale on which tritium moves through its OFC.

Table 10. Comparison of D-T FPP designs for the baseline case and the three possible advanced scenarios. The points refer to the 'moderate' scenarios ($t_d = 2$ yr).

		Baseline	FC	PO	Both
ARC	TBR_r	1.067	1.039	1.017	1.012
	$I_{startup}$ (kg)	1.14	1.12	0.33	0.30
STEP-EBB	TBR_r	1.068	1.040	1.018	1.012
	$I_{startup}$ (kg)	8.94	7.20	2.36	2.20
STEP-Li	TBR_r	1.070	1.041	1.020	1.015
	$I_{startup}$ (kg)	9.15	7.50	2.36	2.20

for regulatory and safety purposes. This will be an important risk analysis for plant designers to consider: I_{res} allows the plant to keep running even if part of the FC breaks temporarily.

Table 11. ARC design parameters, required TBR and start-up inventory for a 'worst-case' scenario.

Parameter	Value	Units
AF	50	%
TBE	0.005	—
f_{DIR}	0	—
t_p	4	h
t_d	2	y
TBR_r	1.35	—
$I_{startup}$	5.4	kg

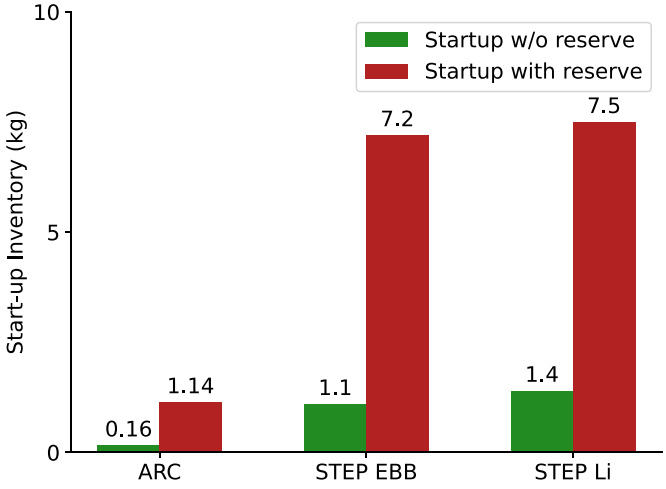

Figure 20. $I_{startup}$ with and without a reserve inventory at the beginning of the operations (FC scenario) for ARC, STEP-EBB and STEP-Li. $I_{startup}$ of high-power-output FPPs is significantly increased if the reserve inventory is included at the beginning of the operations.

However, we will have to consider whether the FC components are the most likely points of failure in the FPP. If the plant is shut down for reasons other than a FC failure, having a large reserve tritium inventory will not turn the plant back on, but it does add potential safety liability.

5.2. Limitations to the maximum TBE in a D-T FPP

The impact of a high TBE on TBR_r and on tritium inventory has been highlighted multiple times in this work. It might seem natural to target extremely high TBE in an FPP. However, a TBE > 10%–20% would be deleterious for the plant economics. In equations (10) and (19) we showed how TBE depends on $f_{He,core}$ (the helium ash fraction in the core), and, via the dilution factor, how P_{fus} (the fusion power density) depends on $f_{He,core}$ [27]. Equations (10) and (19) impose a tradeoff between efficient tritium burn and fusion power density. Figure 21 shows the required TBR and the fusion power density ratio as a function of TBE. The optimal TBE range is between 10% and 15%, depending on the reduction in P_{fus} that is considered acceptable for a given FPP design. An FPP with a very efficient FC (e.g. short t_p and large f_{DIR}) might target relatively low TBE (e.g. TBE = 5%) to maximize P_{fus} and electricity production. Conversely, an FPP with a less efficient FC

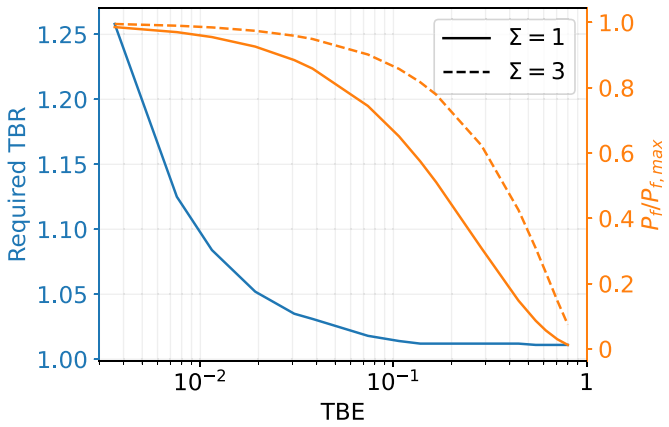

Figure 21. TBR_r and fusion power density ratio as a function of TBE for an ARC-class FPP with baseline parameters ($\eta_{He} = 0.5$, $t_d = 2y$). The fusion power reduction is approximately 30% at TBE = 10% for $\Sigma = 1$, and 10% for $\Sigma = 3$. TBE < 10% is therefore necessary to avoid excessive power reduction at $\Sigma < 3$, while 10% < TBE < 15% might be acceptable for higher Σ.

might choose to maximize TBE, and thus account for smaller revenues from electricity production with a cheaper FC design. The game-changing variable here is the pump selectivity Σ, which allows for a very high TBE with minor drawbacks on the fusion power density if $\Sigma > 3$ [27].

It should be noted that each point plotted in figure 21 represents a distinct FPP design rather than a single design with varying power or TBE (we expect the first generation of FPPs to operate at fixed fusion power). Once P_f is set, the TBE can be chosen according to the FC design and economic considerations. The combination of P_f and TBE sets a $P_{f,max}$, which serves as a design target for the fusion core. This implies that fusion core, divertor and FC are interconnected not only through the gas flows entering and exiting the vacuum chamber, but also by more fundamental relationships among key FPP parameters.

5.3. Potential effect of T trapping in solid components

In this work, we neglected hydrogen trapping and modeled diffusive (or mobile) hydrogen only. Hydrogen can however be trapped in defects of solid materials (vacancies, grain boundaries, impurities, voids, etc) [91, 92]. The concentration of trapped hydrogen depends on the concentration of mobile hydrogen, the material (and its inherent trapping properties), and the temperature. Dark *et al* showed that neglecting trapping in water-cooled lead lithium (WCLL) breeding blankets would lead to an underestimation of the tritium inventory (between 14% and 35% in the structural materials and by a factor of 4.5 in the W FW) [93]. Including trapping will impact the dynamics of the FC models. Components may build up an inventory of trapped hydrogen, delaying tritium retrieval and affecting $I_{startup}$, TBR_r, and/or t_d. Conducting a thorough investigation on hydrogen trapping and its potential influence on the results presented here is outside of the scope of this study as many other parameters need to be determined (trapping properties of materials, solid fraction of components, components temperature distributions, etc). However, this point should be addressed in future work.

5.4. Reducing uncertainty in FC modeling and design

The parametric analysis presented in this work explored ARC and STEP operations across a wide range of possible operating parameters. This range should be narrowed to better focus technology development moving forward. This will require design teams to (1) specify the technologies for the IFC, TES, and HX; (2) obtain better data describing tritium transport phenomena in FLiBe and lithium; (3) quantify the attainable TBE through detailed plasma physics simulations and/or experiments; and (4) refine this model according to the results from (1)–(3).

The first step is a system engineering exercise similar to the one carried out by Day *et al* [94] for the conceptual design of DEMO FC. Existing technologies will probably be implemented in the FC of a First of a kind (FOAK) FPP because of the short timeframe available for development. Residence times at each step of the model can then be better-specified. This step will move the model from technology-agnostic to technology-informed.

Better understanding of tritium transport in FLiBe will be pursued by experiments like LIBRA [31]. Tritium transport properties in FLiBe are affected by large uncertainties [71]. Tritium transport through the IFC and OFC is modeled here by equation (20), but this certainly is too simplistic. Improved datasets describing tritium solubility and permeability through FLiBe and different materials are needed to better predict residence times, improve technologies like the TES, and predict (and mitigate) tritium loss due to permeation of structural materials. For example, LIBRA will investigate tritium transport and radiochemistry in FLiBe in ARC relevant conditions, providing more precise input data to tritium transport models. Tritium extraction methods (gas sparging through salt and sweep gas flowing in tank interstitials) will be tested as well, providing a rough estimate of achievable TES efficiency. Steps like this move the FC model from physics-agnostic to physics-informed.

The third goal will be pursued by devices like SPARC, which will investigate the high-field path to practical fusion energy [19]. Preliminary results for ARC TBE may come even earlier through detailed plasma physics simulations. We know from [1] and the present analysis that the FPP's utilization of fuel has a profound effect on the tritium self-sufficiency of the system. These results will improve confidence in the FC analysis and system design for ARC and STEP.

The last step is a modeling exercise. The FC model is scalable and flexible thanks to its implementation in MATLAB Simulink®. A component level description can be added in a similar way to the one described by Riva *et al* [73] once the uncertainties related to tritium transport properties are reduced. Alternatively, standalone component simulations might be carried out to quantify the tritium residence time. Then, the precise value for τ_i can be implemented in the MATLAB Simulink® model, improving calculation speed.

5.5. Doubling time, construction time, and FPP penetration into the electricity market

In this analysis, the doubling time t_d is defined as the time required to double the FPP's start-up inventory $I_{startup}$. This definition assumes implicitly that the limiting factor on the construction and operation of new FPPs is the availability of tritium fuel for plant start-up. The broader definition of 'doubling time' is the time required to double the number of a given FPP. We refer to this broader definition hereunder as the construction time (t_c) for grid-connected FPP. For the first generation of FPP, t_d and t_c will hardly match. The t_d targets described in this model are affected by large uncertainties. A minimum achievable t_c will remain an unknown data point until the first FPPs are built and operated. However, it is reasonable to expect construction times much longer than the doubling times we targeted in our analysis (i.e. 1 or 2 years). For instance, the median construction time for fission power plants in 2021 was 88 months ($\sim$7.3 yr), despite eight decades of experience building fission power plants [95]. In this paper, we discussed short doubling times: 1 or 2 years. If we optimistically assume a t_c of 6 years for the construction of early FPPs, we see the obvious issue with the aggressive t_d scenarios. A doubling time $t_d \sim 0.3t_c$ sets unnecessarily demanding requirements on the first FPPs without a corresponding advantage in tritium economy. A large amount of tritium would need to be safely stored for years before it could be used. It seems reasonable, then, to target longer t_d for the first generation of FPPs.

However, t_d can be a misleading figure of merit in this context. If the first generation of FPPs demonstrates the technical and economical feasibility of fusion energy production, the construction of many FPP for the second generation might start in parallel, potentially regardless of whether there is immediately tritium available to start the finished plant. We also note that our analysis treats the number of FPPs as a straightforward mathematical variable. In reality, commercial FPPs will be affected by a far more complex political, social, economic, and commercial landscape than can be accounted for in a simple FC analysis. In this work we are considering tritium self-sufficiency for individual FPPs; eventually, we will need to consider what it means for a fusion power sector as a whole to be tritium self-sufficient. As the fusion landscape evolves, we must incorporate more nuanced discussions of fusion economics and future energy scenarios into our understanding of tritium self-sufficiency.

6. Conclusions

The dynamic FC model and analysis of an ARC-class FPP and STEP-class FPPs has been presented in this work. Tritium self-sufficiency was assessed for a wide range of operating parameters and the relative importance of different FC parameters was investigated. Three alternative scenarios (advanced FC, advanced POs, and both) were studied in order to highlight possible R&D paths and design targets.

These results show that tritium self-sufficiency is theoretically achievable in an ARC-class FPP thanks to unique design features, such as demountable coils, replaceable VV and LIB. Low tritium burn efficiencies (TBE $< 1\%$) would require high TBR in the breeding zone ($TBR_r > 1.10$), but the implementation of a direct internal recycling line in this case can lower the TBR_r to easier-to-attain values. For TBE $< 1\%$, lower DIR fractions (e.g. $f_{DIR} = 0.3$) and FPP availability (e.g. AF $= 70\%$) are acceptable from the tritium self-sufficiency standpoint, with $TBR_r < 1.1$. Neutronics analyses of the ARC concept indicate that $TBR_a > TBR_r$ in these scenarios. Research on ARC-relevant plasma physics performance should prioritize achieving TBE $\simeq 1\%$, at a minimum. Similar conclusions apply for STEP-class FPPs. On the engineering side, suitably mature technologies for the FC must be identified or developed.

We showed that doubling time is an effective design target when carrying out FPP tritium self-sufficiency analyses. The choice of t_d has a dramatic impact on tritium self-sufficiency. Very aggressive doubling times, such as $t_d = 1$ yr, will prevent tritium self-sufficiency unless FPPs can achieve relatively high TBE ($>1\%$), most obviously because the TBR_r rapidly becomes physically unobtainable. Relaxing the target doubling time is an effective way to decrease TBR_r. However, doubling time does not exist in a vacuum: it must make sense given projected construction times for new grid-connected FPPs.

Our knowledge of other power plant industries (and of fusion device construction) indicates that FPP construction time is likely to be much longer than 1–2 yr, especially for FOAK plants. FOAK FPPs may target slightly longer doubling times (3–4 yr), making tritium self-sufficiency much easier to achieve, and decreasing the complexity and cost of the plant.

This analysis shows that the required start-up inventory for an ARC-class FPP should meet safety and economics constraints for most operating scenarios considered. Indeed, $I_{startup} < 1$ kg is within reach for an ARC-class FPP if FC technology and plasma performance is sufficiently advanced.

Even a 'worst-case' scenario, with poor system performance and minimal advances in FC technology and plasma performance, results in $I_{startup} < 5$ kg for an ARC-class FPP. This is not the case for STEP designs. STEP's much higher power output will require much larger tritium reserves to balance the risk of fuel cycle failures during the initial stage of plant operation. However, we also discussed how FPPs like STEP can significantly reduce $I_{startup}$ if they are able to tolerate the risk associated with lower tritium reserves. Future analyses of plant reliability should attempt to quantify this risk more explicitly.

In conclusion, the ARC-class fusion power plant is very well positioned with regards to tritium self-sufficiency. It should require a relatively low start-up tritium inventory, be able to maintain relatively low plant inventory, breed and process sufficient tritium to fuel itself, and provide tritium fuel for future plant startup. STEP-class FPPs present more of a challenge when it comes to tritium self-sufficiency, but this analysis indicates that it is achievable.

Finally, we note that this analysis has limitations. The pulsed nature of the FPP and the down times caused by component failures are accounted for at a high level via the availability factor AF, but the model neglects transients involving

FC components (e.g. pump transients) and plasma ramp-up and ramp-down. These transients may impact the dynamics of the system and the performance of the components. As such, the model should be intended as a tool to perform exploratory analyses on FCs, and not as an engineering design tool. The complex physical and chemical processes that govern tritium dynamics in the FC components are described only with the tritium residence time parameter. This provides an effective, but coarse, description of the tritium flow dynamics. Tritium transport in FLiBe is currently under investigation by the LIBRA experiment at the MIT Plasma Science and Fusion Center (PSFC). Expected outcomes from LIBRA will improve the level of detail of the model, allowing for a more accurate prediction of tritium self-sufficiency in ARC-class FPPs.

Acknowledgments

The authors wish to acknowledge the steady support of Kevin B Woller and the MIT PSFC LIBRA team for this project, which aims to develop a pathway by which the scientific goals of the LIBRA initiative can be linked to systems-level analysis. The authors thank the following individuals who provided thoughtful feedback to this work: Mohamad Abdallah of Tokamak Energy, Alexander Creely of Commonwealth Fusion Systems, Randall Field of the MIT Energy Initiative, and Martin Greenwald of the MIT PSFC. The information, data, or work presented herein was funded in part by the Advanced Research Projects Agency-Energy, U.S. Department of Energy, under Award Number DE-AR0001542. The views and opinions of authors expressed herein do not necessarily state or reflect those of the United States Government or any agency thereof. S Meschini acknowledges funding support from Eni S.p.A for his PhD scholarship.

Appendix A. ARC fuel cycle model

A detailed layout of the IFC is shown in figure A.22.
All the quantities used in the residence-time-model are defined in tables A.12 and A.13.

The general form for tritium balance in the ith component is adapted from [1]:

$$\frac{\mathrm{d}I_i}{\mathrm{d}t} = \sum_{j\neq i}\left(f_{j\to i}\frac{I_j}{\tau_j}\right) - (1+\epsilon_i)\left(\frac{I_i}{\tau_i}\right) - \lambda I_i + S_i \tag{A.1}$$

with $\sum_j f_{i\to j} = 1$. The system of ODE that describes the model is:

$$\frac{\mathrm{d}I_1}{\mathrm{d}t} = \mathrm{TBR}\dot{N}_{\mathrm{T,burn}} + \frac{I_3}{\tau_3} + \frac{I_4}{\tau_4} + f_{5-1}\frac{I_5}{\tau_5} - \frac{I_1}{T_1} \tag{A.2}$$

$$\frac{\mathrm{d}I_2}{\mathrm{d}t} = \frac{I_1}{\tau_1} - \frac{I_2}{T_2} \tag{A.3}$$

$$\frac{\mathrm{d}I_3}{\mathrm{d}t} = f_{p-3}\frac{\dot{N}_{\mathrm{T,burn}}}{\mathrm{TBE}} + f_{5-3}\frac{I_5}{\tau_5} - \frac{I_3}{T_3} \tag{A.4}$$

$$\frac{\mathrm{d}I_4}{\mathrm{d}t} = f_{p-4}\frac{\dot{N}_{\mathrm{T,burn}}}{\mathrm{TBE}} + f_{5-4}\frac{I_5}{\tau_5} - \frac{I_4}{T_4} \tag{A.5}$$

$$\frac{\mathrm{d}I_5}{\mathrm{d}t} = (1-\eta_2)\frac{I_2}{\tau_2} - \frac{I_5}{T_5} \tag{A.6}$$

$$\frac{\mathrm{d}I_6}{\mathrm{d}t} = f_{5-6}\frac{I_5}{\tau_5} + f_{9-6}\frac{I_9}{\tau_9} - \frac{I_6}{T_6} \tag{A.7}$$

$$\frac{\mathrm{d}I_7}{\mathrm{d}t} = (1-\mathrm{TBE}-f_{p-3}-f_{p-4})\frac{\dot{N}_{\mathrm{T,burn}}}{\mathrm{TBE}} - \frac{I_7}{T_7} \tag{A.8}$$

$$\frac{\mathrm{d}I_8}{\mathrm{d}t} = (1-f_{\mathrm{DIR}})\frac{I_7}{\tau_7} - \frac{I_8}{T_8} \tag{A.9}$$

$$\frac{\mathrm{d}I_9}{\mathrm{d}t} = \frac{I_6}{\tau_6} + \frac{I_8}{\tau_8} - \frac{I_9}{T_9} \tag{A.10}$$

$$\frac{\mathrm{d}I_{10}}{\mathrm{d}t} = (1-f_{9-6})\frac{I_9}{\tau_9} + f_{\mathrm{DIR}}\frac{I_7}{\tau_7} + \frac{I_{12}}{\tau_{12}} - \frac{\dot{N}_{\mathrm{T,burn}}}{\mathrm{TBE}} - \lambda I_{10} \tag{A.11}$$

$$\frac{\mathrm{d}I_{12}}{\mathrm{d}t} = (1-\eta_2)\frac{I_2}{\tau_2} - \frac{I_{12}}{T_{12}} \tag{A.12}$$

where:

$$\frac{1}{T_i} = \frac{1+\epsilon_i}{\tau_i} + \lambda \tag{A.13}$$

$$\epsilon_i = 10^{-4}, \forall i \neq 3,4,10 \tag{A.14}$$

$$\epsilon_3 = \epsilon_4 = \epsilon_{10} = 0 \tag{A.15}$$

and the initial conditions are given by:

$$I_i(t=0) = 0, \forall i \neq 10 \tag{A.16}$$

$$I_{10}(t=0) = I_{\mathrm{startup}} \tag{A.17}$$

The non-radioactive loss fraction has been assumed as $\epsilon_i = 10^{-4}$ in this work. Nevertheless, it is worth highlighting the impact that this parameter has on the $\mathrm{TBR_r}$. Figure A.24 shows TBR_r for different values of ϵ.

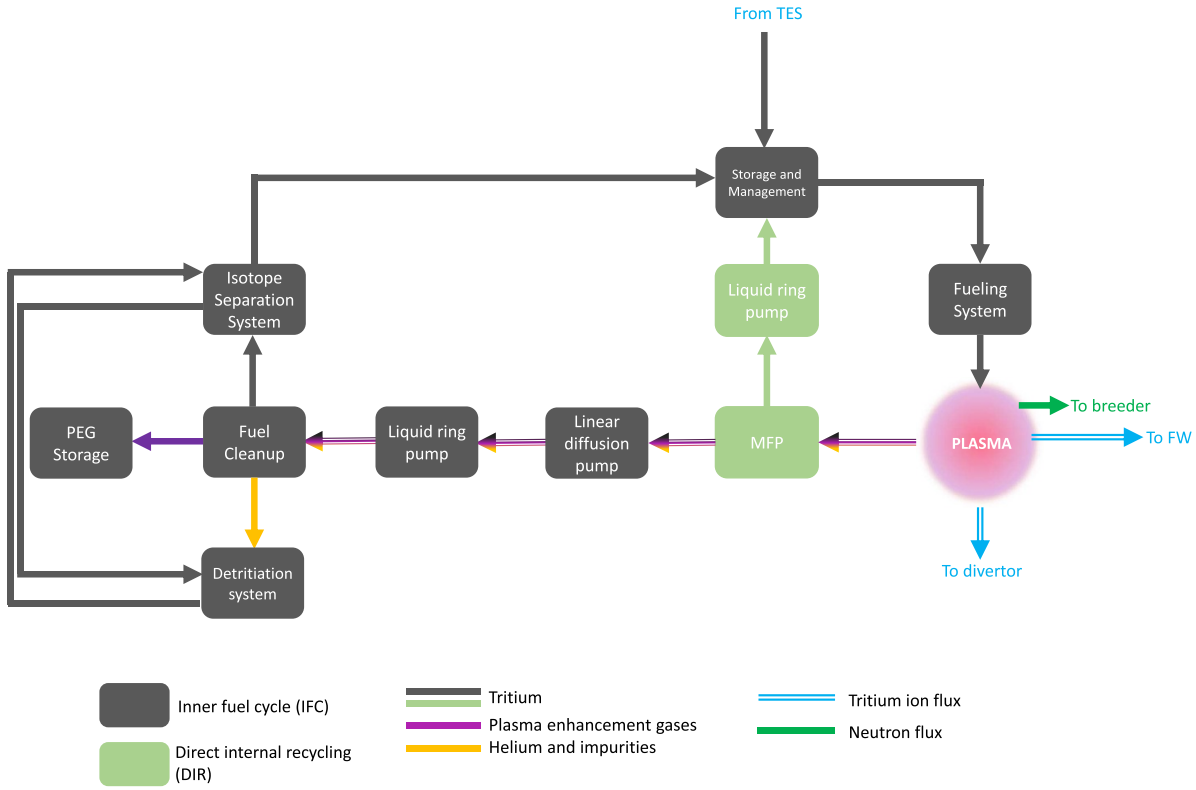

Figure A.22. Detailed layout of ARC IFC considering the DIR loop. Tritium, PEG, helium and impurity flows are shown in different colors.

Table A.12. Mathematical definition of the terms appearing in ARC fuel cycle model (figure A.23).

Component	Flow rate, source or sink
1	$S_1 = \mathrm{TBR}\dot{N}_{\mathrm{T,burn}}$
	$\dot{m}_{5-1} = f_{5-1}\left(\frac{I_5}{\tau_5}\right)$
	$\dot{m}_{3-1} = \frac{I_3}{\tau_3}$
	$\dot{m}_{4-1} = \frac{I_4}{\tau_4}$
	$\dot{m}_{1-2} = -\frac{I_1}{\tau_1}$
2	$\dot{m}_{1-2} = \frac{I_1}{\tau_1}$
	$\dot{m}_{2-12} = -\eta_2 \frac{I_2}{\tau_2}$
	$\dot{m}_{2-5} = -(1-\eta_2)\left(\frac{I_2}{\tau_2}\right)$
3	$\dot{m}_{p-3} = f_{p-3}\frac{\dot{N}_{\mathrm{T,burn}}}{\mathrm{TBE}}$
	$\dot{m}_{5-3} = f_{5-3}\left(\frac{I_5}{\tau_5}\right)$
	$\dot{m}_{3-1} = -\frac{I_3}{\tau_3}$
4	$\dot{m}_{p-4} = f_{p-4}\frac{\dot{N}_{\mathrm{T,burn}}}{\mathrm{TBE}}$
	$\dot{m}_{4-1} = -\frac{I_4}{\tau_4}$
	$\dot{m}_{5-4} = f_{5-4}\frac{I_5}{\tau_5}$
5	$\dot{m}_{2-5} = (1-\eta_2)\left(\frac{I_2}{\tau_2}\right)$
	$\dot{m}_{5-1} = -f_{5-1}\left(\frac{I_5}{\tau_5}\right)$
	$\dot{m}_{5-3} = -f_{5-3}\left(\frac{I_5}{\tau_5}\right)$
	$\dot{m}_{5-4} = -f_{5-4}\frac{I_5}{\tau_5}$
	$\dot{m}_{5-6} = -f_{5-6}\left(\frac{I_5}{\tau_5}\right)$
6	$\dot{m}_{5-6} = f_{5-6}\left(\frac{I_5}{\tau_5}\right)$
	$\dot{m}_{9-6} = f_{9-6}\left(\frac{I_9}{\tau_9}\right)$
	$\dot{m}_{6-9} = -\frac{I_6}{\tau_6}$

(Continued.)

Table A.12. (Continued.)

Component	Flow rate, source or sink
7	$\dot{m}_{p-7} = (1 - \mathrm{TBE} - f_{p-3} - f_{p-4})\frac{\dot{N}_{\mathrm{T,burn}}}{\mathrm{TBE}}$
	$\dot{m}_{7-8} = -(1 - f_{\mathrm{DIR}})\left(\frac{I_7}{\tau_7}\right)$
	$\dot{m}_{7-10} = -f_{\mathrm{DIR}}\left(\frac{I_7}{\tau_7}\right)$
8	$\dot{m}_{7-8} = (1 - f_{\mathrm{DIR}})\left(\frac{I_7}{\tau_7}\right)$
	$\dot{m}_{8-9} = -\frac{I_8}{\tau_8}$
9	$\dot{m}_{6-9} = \frac{I_6}{\tau_6}$
	$\dot{m}_{2-9} = \eta_2\left(\frac{I_2}{\tau_2}\right)$
	$\dot{m}_{8-9} = \frac{I_8}{\tau_8}$
	$\dot{m}_{9-6} = -f_{9-6}\left(\frac{I_9}{\tau_9}\right)$
	$\dot{m}_{9-10} = -(1 - f_{9-6})\left(\frac{I_9}{\tau_9}\right)$
10	$\dot{m}_{9-10} = (1 - f_{9-6})\left(\frac{I_9}{\tau_9}\right)$
	$\dot{m}_{7-10} = f_{\mathrm{DIR}}\left(\frac{I_7}{\tau_7}\right)$
	$\dot{m}_{10-11} = -\frac{\dot{N}_{\mathrm{T,burn}}}{\mathrm{TBE}}$
	$\dot{m}_{12-10} = \frac{I_{12}}{\tau_{12}}$
11	$\dot{m}_{10-11} = \frac{\dot{N}_{\mathrm{T,burn}}}{\mathrm{TBE}}$
	$\dot{m}_{11-p} = -\frac{\dot{N}_{\mathrm{T,burn}}}{\mathrm{TBE}}$
12	$\dot{m}_{2-12} = \eta_2\frac{I_2}{\tau_2}$
	$\dot{m}_{12-10} = -\frac{I_{12}}{\tau_{12}}$
All components	$\mathrm{Losses} = -\epsilon_i\left(\frac{I_i}{\tau_i}\right) - \lambda I_i$

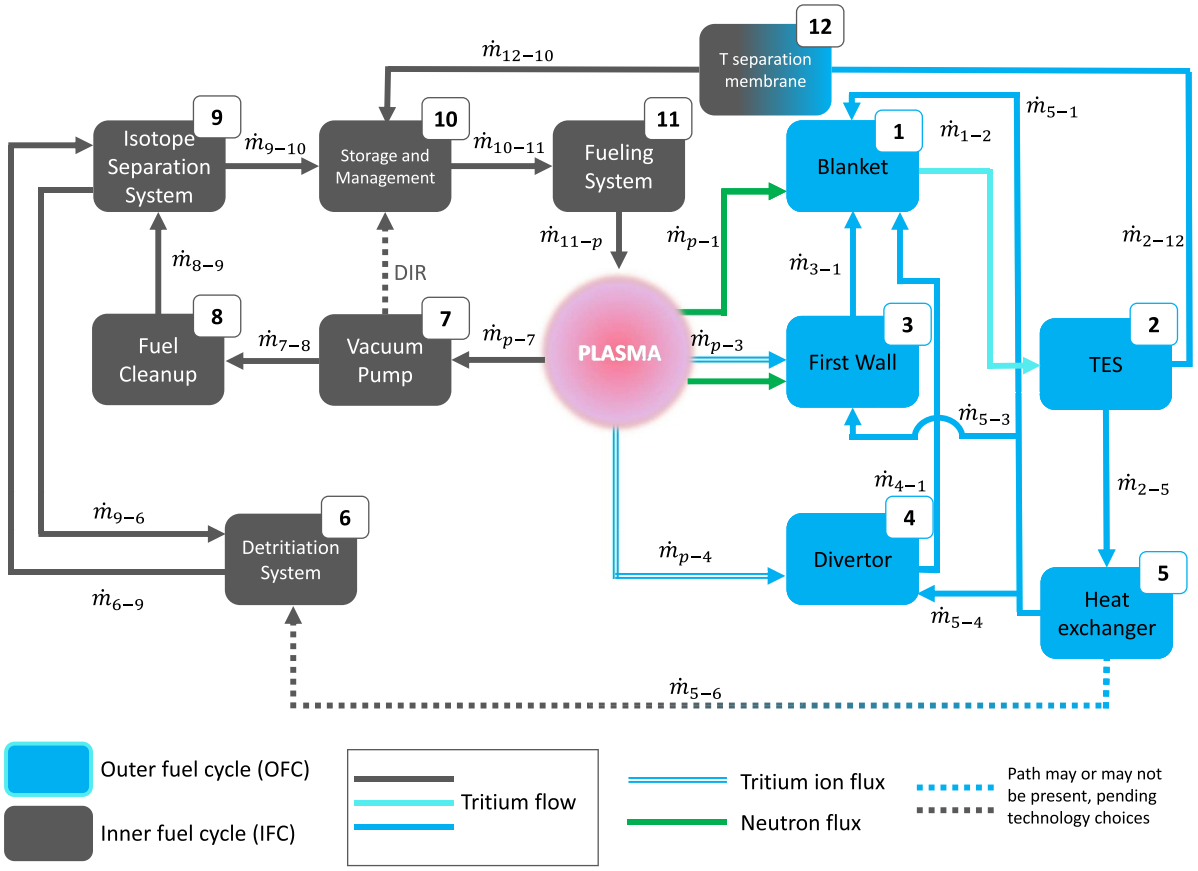

Figure A.23. ARC fuel cycle layout. Only the components that have been modeled are shown in the figure. The tritium flows between components are depicted. For the definition of each tritium flow see table A.12.

Table A.13. Tritium flow rate fractions for the fuel cycle model. The flow rate fractions from the FLiBe tank to the other components have been estimated according to the FLiBe flow rates specified in [13] (∼66% of coolant flow rate to the main chamber, ∼33% to the divertors). An equal distribution from the main chamber to the FW/VV channels and the FLiBe tank was assumed (i.e.$f_{5-3} = f_{5-1}$).

Flow rate fraction	Value
f_{5-1}	0.33
f_{5-3}	0.33
f_{5-6}	10^{-4}
f_{9-6}	0.1
f_{p-3}	10^{-4}
f_{p-4}	10^{-4}

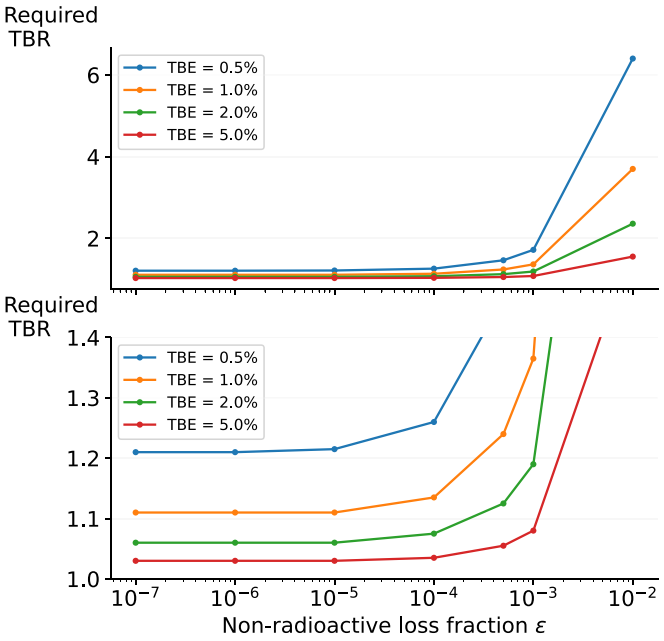

Figure A.24. TBR_r for different values of non-radioactive loss fraction. For $\epsilon > 10^{-3}$ the TBR_r increases up to unattainable values ($TBR_r \gg 1.2$). The bottom plot shows a zoom in the region of interest ($TBR_r < 1.4$).

Appendix B. List of acronyms

ARC	Affordable, Robust, Compact
CANDU	CANadian Deuterium Uranium
CECE	Combined electrolysis and catalytic exchange
CPS	Coolant purification system
DEMO	DEMOnstration nuclear FPP
DIR	Direct internal recycling
EBB	Encapsulated Breeding blanket
FLiBe	$2LiF + BeF_2$
FOAK	First of a kind
FPP	Fusion power plant
FPY	Full power year
FW	First wall
GPR	Gaussian process regression
HX	Heat exchanger
JET-ILW	Joint European Torus—ITER like wall
IFC	Inner fuel cycle
ISS	Isotope separation system
LIB	Liquid immersion blanket
LLE	Liquid–liquid extraction
MFP	Metal foil pump
ODE	Ordinary differential equation
OFC	Outer fuel cycle
PAV	Permeator against vacuum
PFC	Plasma facing component
RAMI	Reliability, availability, maintenability and inspectability
RTM	Residence time method
STEP	Spherical Tokamak for Energy Production
TBR	Tritium breeding ratio
TES	Tritium extraction system
TSS	Tritium self-sufficiency
VV	Vacuum vessel

Appendix C. List of variables

AF	Availability factor (−)
a	Plasma semi-minor radius (m)
B_0	Toroidal magnetic field (T)
B_{max}	Peak on-coil magnetic field (T)
ϵ_i	Fraction of tritium lost from non-radioactive phenomena in the ith component (−)
η_f	Fueling efficiency (−)
η_{TES}	Tritium extraction efficiency
f_{DIR}	Direct internal recycling fraction (−)
κ	Plasma elongation (−)
I_i	Tritium inventory in the ith component (kg)
I_{fus}	Reactivity fusion integral as defined in [85]
I_{opt}	Optimal start-up inventory (kg)
I_{res}	Reserve inventory (kg)
$I_{startup}$	Start-up inventory (kg)
λ	Tritium decay rate ($1\,s^{-1}$)
$\dot{m}$	Tritium mass flow rate ($kg\,s^{-1}$)
MTBF	Mean time between failures (s)
MTTR	Mean time to repair (s)
n	Plasma density (m^{-3})
$\dot{N}_{T,burn}$	Tritium burn rate ($kg\,s^{-1}$)
$\dot{N}_\alpha$	α particles production rate in the core plasma ($kg\,s^{-1}$)
$\dot{N}_{T,in}$	Tritium injected in the vacuum chamber ($kg\,s^{-1}$)
$\dot{N}_{T,div}$	Tritium exhausted by the divertor pumps ($kg\,s^{-1}$)
$\dot{N}_{He,div}$	Helium exhausted by the divertor pumps ($kg\,s^{-1}$)
P_{fus}	Fusion power (MW_{th})
PT	Payback time (s)
q	Fraction of fuel cycle failing (−)
R	Particle recycling coefficient (−)
RIC	Relative sensitivity index coefficient (−)
R_0	Major radius (m)
Σ	Helium selectivity of the divertor pump
t	Time (s)
τ_{BZ}	Tritium residence time in the breeding zone (s)

τ_i	Tritium residence time in the *i*th component (s)
t_c	Construction time for grid-connected FPPs (y)
t_d	Doubling time (y)
τ_p	Particle recycling time (s)
T	Temperature (K)
TBE	Tritium burn efficiency in plasma (−)
TBR	Tritium breeding ratio (−)
TBR_r	Required TBR (−)
TBR_a	Achievable TBR (−)
V_p	Plasma volume (m^3)

ORCID iDs

Samuele Meschini https://orcid.org/0000-0001-8014-903X
Sara E. Ferry https://orcid.org/0000-0002-7505-9571
Rémi Delaporte-Mathurin https://orcid.org/0000-0003-1064-8882

References

[1] Abdou M., Riva M., Ying A., Day C., Loarte A., Baylor L.R., Humrickhouse P., Fuerst T.F. and Cho S. 2020 Physics and technology considerations for the deuterium–tritium fuel cycle and conditions for tritium fuel self sufficiency *Nucl. Fusion* **61** 013001
[2] Sorbom B. *et al* 2014 ARC: a compact, high-field, disassemblable fusion nuclear science facility and demonstration power plant *APS Division of Plasma Physics Meeting Abstracts* (*New Orleans, Louisiana, USA,* 27–31 *October 2014*) vol 2014 p T8-005 (available at: https://meetings.aps.org/Meeting/DPP14/Session/TP8.5)
[3] Fradera J., Sádaba S., Calvo F., Ha S., Merriman S., Gordillo P., Connell J., Elfaraskoury A. and Echeveste B. 2021 Pre-conceptual design of an encapsulated breeder commercial blanket for the STEP fusion reactor *Fusion Eng. Des.* **172** 112909
[4] Schoofs F. and Todd T.N. 2022 Magnetic field and power consumption constraints for compact spherical tokamak power plants *Fusion Eng. Des.* **176** 113022
[5] Peng Y.-K.M. and Strickler D.J. 1986 Features of spherical torus plasmas *Nucl. Fusion* **26** 769
[6] Wilson H.R. *et al* 2004 Integrated plasma physics modelling for the Culham steady state spherical tokamak fusion power plant *Nucl. Fusion* **44** 917
[7] Ono M. and Kaita R. 2015 Recent progress on spherical torus research *Phys. Plasmas* **22** 040501
[8] Sykes A. (The START Team, The NBI Team, The MAST Team and The Theory Team) 1999 The spherical tokamak programme at Culham *Nucl. Fusion* **39** 1271
[9] Wilson H., Chapman I., Denton T., Morris W., Patel B., Voss G. and Waldon C. (The STEP Team) 2020 STEP–on the pathway to fusion commercialization *Commercialising Fusion Energy: How Small Businesses are Transforming big Science* (IOP Publishing)
[10] Bocci B., Hartwig Z., Segantin S., Testoni R., Whyte D. and Zucchetti M. 2020 ARC reactor materials: activation analysis and optimization *Fusion Eng. Des.* **154** 111539
[11] Segantin S., Testoni R., Hartwig Z., Whyte D. and Zucchetti M. 2020 Optimization of tritium breeding ratio in ARC reactor *Fusion Eng. Des.* **154** 111531
[12] Segantin S., Testoni R. and Zucchetti M. 2019 The lifetime determination of ARC reactor as a load-following plant in the energy framework *Energy Policy* **126** 66–75
[13] Kuang A.Q. *et al* 2018 Conceptual design study for heat exhaust management in the ARC fusion pilot plant *Fusion Eng. Des.* **137** 221–42
[14] Ferrero G., Meschini S. and Testoni R. 2022 A preliminary CFD and tritium transport analysis for ARC blanket *Fusion Sci. Technol.* **78** 617–30
[15] Meschini S., Testoni R. and Zucchetti M. 2022 Development of an object-oriented, thermal-hydraulics model for ARC FLiBe loop safety assessment *Fusion Eng. Des.* **178** 113095
[16] Segantin S., Testoni R. and Zucchetti M. 2020 ARC reactor–neutron irradiation analysis *Fusion Eng. Des.* **159** 111792
[17] Bae J.W., Peterson E. and Shimwell J. 2022 ARC reactor neutronics multi-code validation *Nucl. Fusion* **62** 066016
[18] Segantin S., Meschini S., Testoni R. and Zucchetti M. 2022 Preliminary investigation of neutron shielding compounds for ARC-class tokamaks *Fusion Eng. Des.* **185** 113335
[19] Creely A.J. *et al* (The SPARC Team) 2020 Overview of the SPARC tokamak *J. Plasma Phys.* **86** 865860502
[20] Kovari M., Coleman M., Cristescu I. and Smith R. 2017 Tritium resources available for fusion reactors *Nucl. Fusion* **58** 026010
[21] Baylor L.R., Jernigan T.C., Parks P.B., Antar G., Brooks N.H., Combs S.K., Fehling D.T., Foust C.R., Houlberg W.A. and Schmidt G.L. 2007 Comparison of deuterium pellet injection from different locations on the DIII-D tokamak *Nucl. Fusion* **47** 1598
[22] Kirk Combs S.K., Baylor L.R., Meitner S.J., Caughman J.B.O., Rasmussen D.A. and Maruyama S. 2012 Overview of recent developments in pellet injection for ITER *Fusion Eng. Des.* **87** 634–40
[23] Fischer U., Boccaccini L.V., Cismondi F., Coleman M., Day C., Hörstensmeyer Y., Moro F. and Pereslavtsev P. 2020 Required, achievable and target TBR for the european DEMO *Fusion Eng. Des.* **155** 111553
[24] Pearson R.J., Antoniazzi A.B. and Nuttall W.J. 2018 Tritium supply and use: a key issue for the development of nuclear fusion energy *Fusion Eng. Des.* **136** 1140–8
[25] Day C and Giegerich T 2013 The direct internal recycling concept to simplify the fuel cycle of a fusion power plant *Fusion Eng. Des.* **88** 616–20
[26] Groth M. *et al* 2002 Helium and neon enrichment studies in the JET mark IIAP and mark IIGB divertors *Nucl. Fusion* **42** 591
[27] Whyte D.G., Ferry S.E., Meschini S. and Delaporte-Mathurin R. 2023 Tritium burn efficiency in deuterium-tritium magnetic fusion *Nucl. Fusion* (https://doi.org/10.1088/1741-4326/acf3fb)
[28] Goetz J.A., Lipschultz B., Pitcher C.S., Terry J.L., Bonoli P.T., Rice J.E. and Wukitch S.J. 1999 Impurity compression and enrichment studies on alcator C-MOD *J. Nucl. Mater.* **266** 354–9
[29] Sakasai A. *et al* 1999 Helium exhaust in ELMy H-mode plasmas with W-shaped pumped divertor of JT-60U *J. Nucl. Mater.* **266** 312–7
[30] Hartwig Z.S. *et al* 2020 Viper: an industrially scalable high-current high-temperature superconductor cable *Supercond. Sci. Technol.* **33** 11LT01
[31] Ferry S.E., Woller K.B., Peterson E.E., Sorensen C. and Whyte D.G. 2022 The LIBRA experiment: investigating robust tritium accountancy in molten FLiBe exposed to a D-T fusion neutron spectrum *Fusion Sci. Technol.* **79** 13–35
[32] Forsberg C.W., Lam S., Carpenter D.M., Whyte D.G., Scarlat R., Contescu C., Wei L., Stempien J. and Blandford E. 2017 Tritium control and capture in salt-cooled fission and fusion reactors: status,

challenges and path forward *Nucl. Technol.* **197** 119–39
[33] Nordlund K., Björkas C., Ahlgren T., Lasa A. and Elisabet Sand A.E. 2014 Multiscale modelling of plasma–wall interactions in fusion reactor conditions *J. Phys. D: Appl. Phys.* **47** 224018
[34] Causey R.A. 2002 Hydrogen isotope retention and recycling in fusion reactor plasma-facing components *J. Nucl. Mater.* **300** 91–117
[35] Widdowson A. *et al* 2017 Overview of the JET ITER-like wall divertor *Nucl. Mater. Energy* **12** 499–505
[36] Hirohata Y. *et al* 2004 Depth profile and retention of hydrogen isotopes in graphite tiles used in the W-shaped divertor of JT-60U *J. Nucl. Mater.* **329** 785–9
[37] Rohde V., Mayer M., Mertens V., Neu R. and Sugiyama K. (The ASDEX Upgrade Team) 2009 Dynamic and static deuterium inventory in ASDEX upgrade with tungsten first wall *Nucl. Fusion* **49** 085031
[38] Peters B.J., Hanke S. and Day C. 2018 Metal foil pump performance aspects in view of the implementation of direct internal recycling for future fusion fuel cycles *Fusion Eng. Des.* **136** 1467–71
[39] Giegerich T. and Day C. 2014 The KALPUREX-process–a new vacuum pumping process for exhaust gases in fusion power plants *Fusion Eng. Des.* **89** 1476–81
[40] Cristescu I., Priester F., Rapisarda D., Santucci A. and Utili M. 2020 Overview of the tritium technologies for the EU DEMO breeding blanket *Fusion Sci. Technol.* **76** 446–57
[41] Brezinsek S. *et al* (JET-EFDA contributors) 2015 Plasma-surface interaction in the Be/W environment: conclusions drawn from the JET-ILW for ITER *J. Nucl. Mater.* **463** 11–21
[42] Maurizio R., Elmore S., Fedorczak N., Gallo A., Reimerdes H., Labit B., Theiler C., Tsui C.K. and Vijvers W.A.J. (The TCV Team and The MST1 Team) 2017 Divertor power load studies for attached l-mode single-null plasmas in TCV *Nucl. Fusion* **58** 016052
[43] Petrie T.W. *et al* 2019 High performance double-null plasmas under radiating divertor and mantle scenarios on DIII-D *Nucl. Fusion* **59** 086053
[44] Reimerdes H. *et al* 2013 Power distribution in the snowflake divertor in TCV *Plasma Phys. Control. Fusion* **55** 124027
[45] Martelli E., Giannetti F., Caruso G., Tarallo A., Polidori M., Barucca L. and Del Nevo A. 2018 Study of EU DEMO WCLL breeding blanket and primary heat transfer system integration *Fusion Eng. Des.* **136** 828–33
[46] Kern D.Q. and Kern D.Q. 1950 *Process Heat Transfer* vol 5 (McGraw-Hill)
[47] Zohuri B. 2011 *Heat Pipe Design and Technology* (Springer)
[48] Papa F., Utili M., Venturini A., Caruso G., Savoldi L., Bonifetto R., Valerio D., Allio A., Collaku A. and Tarantino M. 2021 Engineering design of a permeator against vacuum mock-up with niobium membrane *Fusion Eng. Des.* **166** 112313
[49] Garcinuno B., Rapisarda D., Fernández I., Moreno C., Palermo I. and Ibarra A. 2017 Design of a permeator against vacuum for tritium extraction from eutectic lithium-lead in a DCLL DEMO *Fusion Eng. Des.* **117** 226–31
[50] Humrickhouse P.W. and Merrill B.J. 2015 Vacuum permeator analysis for extraction of tritium from DCLL blankets *Fusion Sci. Technol.* **68** 295–302
[51] Maroni V.A., Wolson R.D. and Staahl G.E. 1975 Some preliminary considerations of a molten-salt extraction process to remove tritium from liquid lithium fusion reactor blankets *Nucl. Technol.* **25** 83–91
[52] Satoshi F., Masabumi N. and Akio S. 2001 Calculation of recovery rates of tritium from FLiBe blanket *Fusion Technol.* **39** 1073–7
[53] Okino F., Noborio K., Yamamoto Y. and Konishi S. 2012 Vacuum sieve tray for tritium extraction from liquid Pb–17Li *Fusion Eng. Des.* **87** 1014–8
[54] Day C., Antipenkov A., Dremel M., Haas H., Hauer V., Mack A., Murdoch D.K. and Wykes M. 2007 R&D and design for the cryogenic and mechanical vacuum pumping systems of ITER *Vacuum* **81** 738–47
[55] Giegerich T. and Day C. 2013 Conceptuation of a continuously working vacuum pump train for fusion power plants *Fusion Eng. Des.* **88** 2206–9
[56] Giegerich T., Day C. and Jäger M. 2017 Mercury ring pump proof-of-principle testing in the THESEUS facility *Fusion Eng. Des.* **124** 809–13
[57] Bornschein B., Glugla M., Günther K., Lässer R., Le T.L., Simon K.H. and Welte S. 2003 Tritium tests with a technical PERMCAT for final clean-up of ITER exhaust gases *Fusion Eng. Des.* **69** 51–56
[58] Kotoh K., Tanaka M., Takashima S., Tsuge T., Asakura Y., Uda T. and Sugiyama T. 2010 Verification of hydrogen isotope separation/enrichment by pressure swing adsorption process: successive enrichment of deuterium using SZ-5A column *Fusion Eng. Des.* **85** 1992–8
[59] Xiao X., Sessions H.T. and Rabun R. 2022 Advanced isotope separation technology for fusion fuel *Fusion Sci. Technol.* **78** 253–7
[60] Ana G. *et al* 2016 Construction and commissioning of a hydrogen cryogenic distillation system for tritium recovery at ICIT Rm. Valcea *Fusion Eng. Des.* **106** 51–55
[61] Ducret D., Ballanger A., Steimetz J., Laquerbe C., Baudouin O. and Sere Peyrigain P. 2001 Hydrogen isotopes separation by thermal cycling absorption process *Fusion Eng. Des.* **58** 417–21
[62] Perevezentsev A.N., Andreev B.M., Rozenkevich M.B., Pak Y.S., Ovcharov A.V. and Marunich S.A. 2010 Wet scrubber technology for tritium confinement at ITER *Fusion Eng. Des.* **85** 1206–10
[63] Hammerli M., Stevens W.H. and Butler J.P. 1978 *Combined Electrolysis Catalytic Exchange (CECE) Process for Hydrogen Isotope Separation* (ACS Publications)
[64] Alekseev I.A., Bondarenko S.D., Fedorchenko O.A., Vasyanina T.V., Konoplev K.A., Arkhipov E.A., Voronina T.V., Grushko A.I., Tchijov A.S. and Uborsky. V.V. 2003 Heavy water detritiation by combined electrolysis catalytic exchange at the experimental industrial plant *Fusion Eng. Des.* **69** 33–37
[65] Shmayda W.T. and Mayer P. 1984 Uranium beds for temporary tritium storage *J. Less-Common Met.* **104** 239–50
[66] Shmayda W.T., Heics A.G. and Kherani N.P. 1990 Comparison of uranium and zirconium cobalt for tritium storage *J. Less-Common Met.* **162** 117–27
[67] Longhurst G.R. 1988 Pyrophoricity of tritium-storage bed materials *Fusion Technol.* **14** 750–5
[68] Wallace W.E., Karlicek R.F. and Imamura H. 1979 Mechanism of hydrogen absorption by lanthanum-nickel (LaNi5) *J. Phys. Chem.* **83** 1708–12
[69] Combs S.K. 1993 Pellet injection technology *Rev. Sci. Instrum.* **64** 1679–98
[70] Abdou M.A., Vold E.L., Gung C.Y., Youssef M.Z. and Shin K. 1986 Deuterium-tritium fuel self-sufficiency in fusion reactors *Fusion Technol.* **9** 250–85
[71] Humrickhouse P.W. and Fuerst T.F. 2020 Tritium transport phenomena in molten-salt reactors *Technical Report* (Idaho National Lab. (INL))
[72] Ying A., Zhang H., Merrill B., Ahn M.-Y. and Cho S. 2018 Breeding blanket system design implications on tritium transport and permeation with high tritium ion

implantation: a MATLAB/Simulink, COMSOL integrated dynamic tritium transport model for HCCR TBS *Fusion Eng. Des.* **136** 1153–60
[73] Riva M., Ying A., Abdou M., Ahn M.-Y. and Cho S. 2019 Impact of outer fuel cycle tritium transport on initial start-up inventory for next fusion devices *Fusion Sci. Technol.* **75** 1037–45
[74] Coleman M., Hörstensmeyer Y. and Cismondi F. 2019 DEMO tritium fuel cycle: performance, parameter explorations and design space constraints *Fusion Eng. Des.* **141** 79–90
[75] Meschini S. 2023 SamueleMeschini/fuel-cycle: submitted version (Zenodo) (https://doi.org/10.5281/zenodo.8019892)
[76] Hamby D.M. 1994 A review of techniques for parameter sensitivity analysis of environmental models *Environ. Monit. Assess.* **32** 135–54
[77] Zucchetti M., Hartwig Z., Meschini S., Segantin S., Testoni R. and Whyte D. 2021 ARC reactor: radioactivity safety assessment and preliminary environmental impact study *Fusion Eng. Des.* **162** 112132
[78] Mignacca B. and Locatelli G. 2020 Economics and finance of molten salt reactors *Prog. Nucl. Energy* **129** 103503
[79] U.S. Energy Information Administration (EIA) 2022 Electric power monthly, average price of electricity to ultimate customers by end-use sector (available at: www.eia.gov/electricity/monthly/epm_table_grapher.php?t=epmt_5_6_a) (Accessed 21 September 2022)
[80] Abdou M., Morley N.B., Smolentsev S., Ying A., Malang S., Rowcliffe A. and Ulrickson M. 2015 Blanket/first wall challenges and required R&D on the pathway to DEMO *Fusion Eng. Des.* **100** 2–43
[81] Anderson J.L. *et al* 1988 Experience of TSTA milestone runs with 100 grams-level of tritium *Fusion Technol.* **14** 438–43
[82] Fukada S., Nishikawa M., Sagara A. and Terai T. 2002 Mass-transport properties to estimate rates of tritium recovery from Flibe blanket *Fusion Sci. Technol.* **41** 1054–8
[83] Calderoni P., Sharpe P., Hara M. and Oya Y. 2008 Measurement of tritium permeation in Flibe (2LiF–BeF2) *Fusion Eng. Des.* **83** 1331–4
[84] Cismondi F. *et al* 2020 Progress of the conceptual design of the european DEMO breeding blanket, tritium extraction and coolant purification systems *Fusion Eng. Des.* **157** 111640
[85] Jackson G.L., Chan V.S. and Stambaugh R.D. 2013 An analytic expression for the tritium burnup fraction in burning-plasma devices *Fusion Sci. Technol.* **64** 8–12
[86] Davison H.W. 1968 *Compilation of Thermophysical Properties of Liquid Lithium* vol 4650 (National Aeronautics and Space Administration)
[87] Smolentsev S., Morley N. and Abdou M. 2005 Code development for analysis of MHD pressure drop reduction in a liquid metal blanket using insulation technique based on a fully developed flow model *Fusion Eng. Des.* **73** 83–93
[88] Williams C. and Rasmussen C. 1995 Gaussian processes for regression *Advances in Neural Information Processing Systems* vol 8 (MIT Press)
[89] Smith F.J., Land J.F., Begun G.M. and La Gamma de Batistoni A.M. 1979 The solubility and isotopic exchange equilibrium for hydrogen isotopes in lithium *J. Inorg. Nucl. Chem.* **41** 1001–9
[90] Aiello A., Ciampichetti A. and Benamati G. 2006 Determination of hydrogen solubility in lead lithium using sole device *Fusion Eng. Des.* **81** 639–44
[91] Delaporte-Mathurin R. *et al* 2021 Fuel retention in WEST and ITER divertors based on FESTIM monoblock simulations *Nucl. Fusion* **61** 126001
[92] Hodille E. 2016 Study and modeling of the deuterium trapping in ITER relevant materials *PhD Thesis* Aix-Marseille
[93] Dark J., Delaporte-Mathurin R., Charles Y., Hodille E.A., Grisolia C. and Mougenot J. 2021 Influence of hydrogen trapping on WCLL breeding blanket performances *Nucl. Fusion* **61** 116076
[94] Day C., Butler B., Giegerich T., Lang P.T., Lawless R. and Meszaros B. 2016 Consequences of the technology survey and gap analysis on the EU DEMO R&D programme in tritium, matter injection and vacuum *Fusion Eng. Des.* **109** 299–308
[95] World Nuclear Association 2022 *World Nuclear Performance Report 2022* (available at:www.world-nuclear.org/getmedia/9dafaf70-20c2-4c3f-ab80-f5024883d9da/World-Nuclear-Performance-Report-2022.pdf.aspx) (Accessed 24 February 2023)